ORGANOMETALLICS

Article

pubs.acs.org/Organometallics

Synthesis and Reactivity of Palladium(II) Alkyl Complexes that Contain Phosphine-cyclopentanesulfonate Ligands

Rebecca E. Black and Richard F. Jordan*

Department of Chemistry, The University of Chicago, 5735 South Ellis Avenue, Chicago, Illinois 60637, United States

Supporting Information

ABSTRACT: The synthesis of the phosphine-cyclopentanesulfonate pro-ligands Li/K[2-PPh_2-cyclopentanesulfonate] (Li/K[**2a**]), Li/K[2-P(2-OMe-Ph)$_2$-cyclopentanesulfonate] (Li/K[**2b**]), and H[**2b**], and the corresponding Pd(II) alkyl complexes (κ^2-*P,O*-**2a**)PdMe(pyridine) (**3a**) and (κ^2-*P,O*-**2b**)PdMe(pyridine) (**3b**) is described. The sulfonate-bridged base-free dimer {(**2b**)PdMe}$_2$ (**4b**) was synthesized by abstraction of pyridine from **3b** using $B(C_6F_5)_3$. The borane-coordinated base-free dimer [{**2b**·$B(C_6F_5)_3$}PdMe]$_2$ (**5b**), in which $B(C_6F_5)_3$ binds to a sulfonate oxygen, was prepared by addition of 1 equiv of $B(C_6F_5)_3$ per Pd to **4b** or addition of 2 equiv of $B(C_6F_5)_3$ to **3b**. Compounds **3b**, **4b**, and **5b** polymerize ethylene with low activity (up to 210 kg mol^{-1} h^{-1} at 250 psi and 80 °C) to linear polyethylene (M_n = 1950−5250 Da) with predominantly internal olefin placements. **3b** and **4b** copolymerize ethylene with methyl acrylate to linear copolymers that contain up to 11.7 mol % methyl acrylate, which is incorporated as $-CH_2CH(CO_2Me)CH_2-$ (80%) in-chain units and $-CH_2CH(CO_2Me)Me$ (8%) and $-CH_2CH{=}CH(CO_2Me)$ (12%) chain-end units. **3b** and **4b** also copolymerize ethylene with vinyl fluoride to linear copolymers that contain up to 0.41 mol % vinyl fluoride, which is incorporated as $-CH_2CHFCH_2-$ (~80%) in-chain units and $-CH_2CF_2H$ (7%), $-CH_2CHFCH_3$ (5%), and $-CH_2CH_2F$ (8%) chain-end units. Complexes **3b** and **4b** are more stable and active in ethylene polymerization than analogous (PAr_2-$CH_2CH_2SO_3$)PdR catalysts, but are less active than analogous (PAr_2-*arene*sulfonate)PdR catalysts. Low-temperature NMR studies show that **4b** reacts with ethylene below −10 °C to form the ethylene adduct *cis-P,R*-(**2b**)PdMe(ethylene) (**7b**), which undergoes ethylene insertion at 5 °C. DFT calculations for a model (PMe_2-cyclopentanesulfonate)Pd(Pr)(ethylene) species show that ethylene insertion proceeds by *cis-P,R*/*trans-P,R* isomerization followed by migratory insertion, and that the lower activity of **3b** and **4b** vis-à-vis analogous (PAr_2-arenesulfonate)PdR catalysts results from a higher barrier for migratory insertion of the *trans-P,R* isomer.

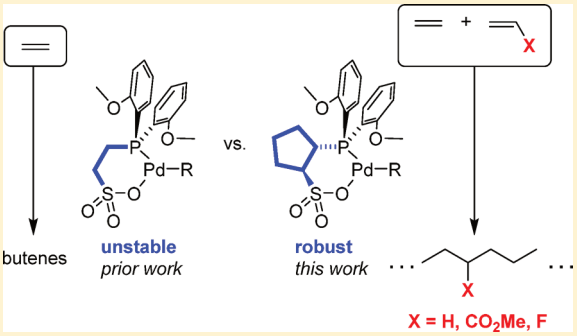

INTRODUCTION

Pd(II) alkyl complexes that contain *ortho*-phosphine-arenesulfonate (PO^-) ligands (**A**, Chart 1) polymerize ethylene to linear polyethylene (PE) and copolymerize ethylene with a wide variety of polar vinyl monomers to functionalized linear PEs.[1−19] While the ability to incorporate diverse comonomers is an advantage of the (PO)PdR system, ethylene polymerization activities and PE molecular weights (MWs) are generally low for these catalysts compared to what is observed for other single-site catalysts,[20,21] and the polar monomers further reduce activities and MWs.

Many electronic and steric modifications of the $-PR_2$ unit of (PO)PdRL catalysts **A** have been explored in efforts to improve the performance of these catalysts.[14,17,22−24] Mecking and co-workers investigated the ethylene polymerization properties of diarylphosphine-benzenesulfonate catalysts (**B**, L = dmso, Chart 1), in which the *para*-R substituent was varied to probe electronic effects.[24] Catalysts with electron-donating substituents produced PE with higher MW but exhibited somewhat lower activity (R = OMe: M_n = 17 000, activity = 2128 kg mol^{-1} h^{-1}) compared to catalysts with electron-withdrawing substituents (R = CF_3: M_n = 8000, activity = 2632 kg mol^{-1} h^{-1}). Nozaki and co-workers examined the polymerization behavior of type-**A** catalysts that incorporate $-P(alkyl)_2$ units of varying size to probe steric effects.[14] Catalysts with more sterically demanding $-PR_2$ units produced PE with higher MW than those with smaller phosphines, likely due to steric blockage of the axial positions of the square-planar metal center (R = ^{i}Pr: M_n = 6700; R = menthyl: M_n = 169 000). Catalyst activity generally increased with increasing steric bulk of the $-PR_2$ unit (R = ^{t}Bu: 1860 kg mol^{-1} h^{-1}) but decreased when the phosphine substituents became too bulky (R = menthyl: 205 kg mol^{-1} h^{-1}). Claverie and co-workers compared the ethylene polymerization performance of type-**A** complexes with a range of $-PAr_2$, $-P(alkyl)_2$ and $-PAr(alkyl)$ units (L = pyridine or lutidine, Chart 1).[22] While no clear relationship between the size of the $-PR_2$ unit and the MW of the PE emerged, a strong positive correlation between the phosphine donor ability, as assessed by the BE(B) descriptor within the

Received: July 27, 2017
Published: August 23, 2017

DOI: 10.1021/acs.organomet.7b00572
Organometallics 2017, 36, 3415−3428

Chart 1. (PO)PdR Complexes

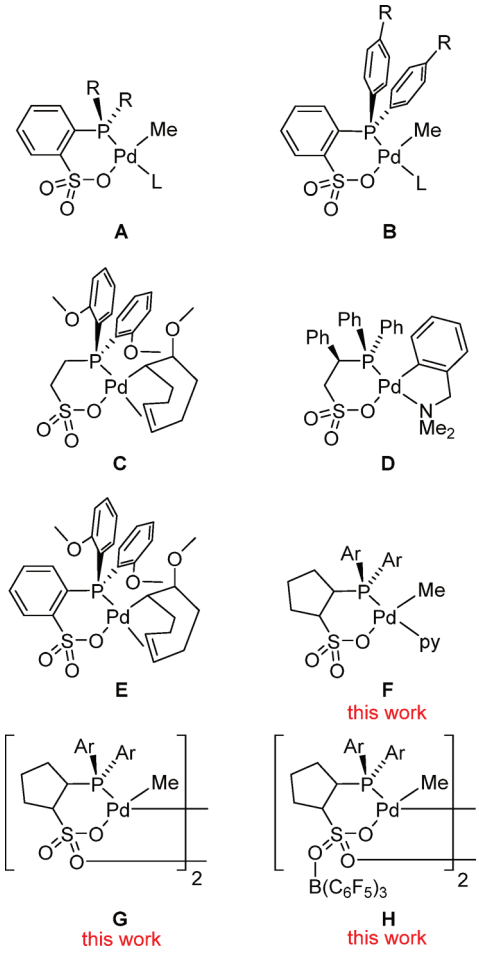

ligand knowledge base for monodentate P donors (LKB-P),[25] and catalyst activity was observed.

Mecking and co-workers analyzed the performance of type-**A** complexes with a range of $-PAr_2$ units in ethylene/methyl acrylate (MA) copolymerization.[17] Catalysts with more strongly electron-donating phosphines were less active but did not deactivate as quickly as catalysts with less electron-donating phosphines, and sterically crowded catalysts produced copolymers with higher MW than did sterically open catalysts. Claverie and co-workers noted that while type-**A** catalysts with $-PR_2 = -P(^tBu)_2$ or $-PPh^tBu$ are both very active for ethylene homopolymerization, the latter incorporates MA much more effectively than the former.[22] This difference was ascribed to steric effects.

The marked dependence of the behavior of (PR_2-arenesulfonate)PdR catalysts on the structure of the PR_2 unit suggests that replacement of the arene linker in type-**A** catalysts with an alkane linker may also strongly influence catalyst performance.[26] However, to date, only a few phosphine-alkanesulfonate ligands[27,28] and Pd^{II} alkyl complexes thereof (**C**[29] and **D**,[30] Chart 1) have been reported. (PAr_2-$CH_2CH_2SO_3$)PdR complex **C** oligomerizes ethylene to butenes and hexenes but rapidly degrades to catalytically inactive species.[31] Compound **C** also catalyzes the nonalternating copolymerization of ethylene and CO but is less active and produces polyketones with lower MW and fewer nonalternating ethylene units compared to the benzene-linked analogue **E**.[29,31] The reactivity of **D** has not been reported.[30]

The low stability of the presumed active {P(2-OMe-Ph)$_2$$CH_2CH_2SO_3$}PdR species derived from **C** is likely due to the high skeletal flexibility that results from facile rotation around the PC−CS bond. As shown in Scheme 1, dissociation

Scheme 1. Proposed Decomposition Pathways

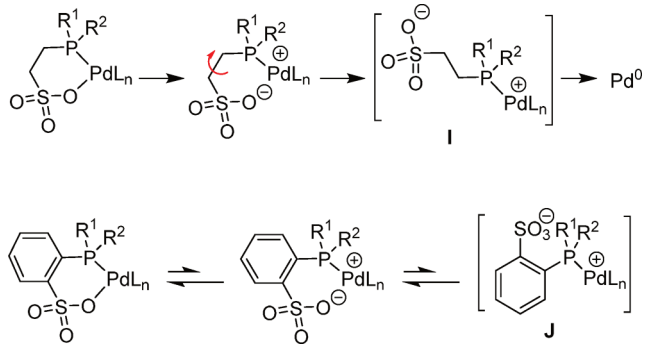

of the sulfonate ligand and rotation around the PC−CS bond would generate κ^1-PO species **I**, which is expected to decompose to Pd^0. In contrast, if sulfonate decoordination occurs in the arene-linker case, then recoordination is favored because rotation around the PC−CS bond is not possible. Rotation around the C(Ar^{SO3})−P bond could lead to κ^1-species **J**, but it is likely to have a barrier of 10−15 kcal/mol.[18,32] Thus, sulfonate recoordination is favored.[33,34] To date, decoordination of the sulfonate oxygen in a (diarylphosphine-arenesulfonate)Pd species has only been observed in the presence of an excess of strong Lewis base. For example, the reaction of [{2-P(2-OMe-Ph)$_2$-benzenesulfonate}Pd(py)$_2$][SbF_6] and pyridine generates [{κ^1-*P*-2-P(2-OMe-Ph)$_2$-benzenesulfonate}Pd(py)$_3$][SbF_6], but this reaction is reversible.[35] Even coordination of the strong Lewis acid $B(C_6F_5)_3$ to the sulfonate group does not cleave the Pd−sulfonate bond.[36]

One potential strategy for stabilizing (diarylphosphine-alkanesulfonate)PdRL compounds is to incorporate a cyclic alkane linker to preclude PC−CS bond rotation. Here, we report the synthesis of two 2-diarylphosphine-*cyclopentane*sulfonate ligands (C5-PO^-) and the corresponding Pd(II) complexes (C5-PO)PdMe(py) (**F**), {(C5-PO)PdMe}$_2$ (**G**), and {(C5-PO·$B(C_6F_5)_3$)PdMe}$_2$ (**H**, Chart 1). We also describe the behavior of these complexes in ethylene polymerization and ethylene copolymerization with methyl acrylate (MA) and vinyl fluoride (VF).

RESULTS AND DISCUSSION

Diarylphosphine-cyclopentanesulfonate Ligands (C5-PO^-). Salts of 2-diarylphosphine-cyclopentanesulfonate ligands that contain $-PPh_2$ (Li/K[**2a**]) or $-P$(2-OMe-Ph)$_2$ (Li/K[**2b**]) units were synthesized according to Scheme 2. K[*trans*-2-Br-cylopentanesulfonate] (K[**1**]) was prepared by nucleophilic opening of cyclopentane-β-sultone[37] by [NBu_4]Br followed by aqueous salt exchange with K[PF_6]. The *trans* orientation of K[**1**] was established by quantitative $^1H-^1H$ NOESY experiments and X-ray diffraction analysis of [K(18-*crown*-6)][**1**] (Figure 1). The reaction of K[**1**] with the appropriate lithium phosphide[38−41] gave *trans*-Li/K[**2a**] and *trans*-Li/K[**2b**]. The amount of Li^+ and K^+ in Li/K[**2a**] was quantified by ICP-MS.

The retention of stereochemistry in these substitution reactions likely results from anchimeric assistance by the

DOI: 10.1021/acs.organomet.7b00572
Organometallics 2017, 36, 3415−3428

Scheme 2. PAr_2-cyclopentanesulfonate Ligand Synthesis

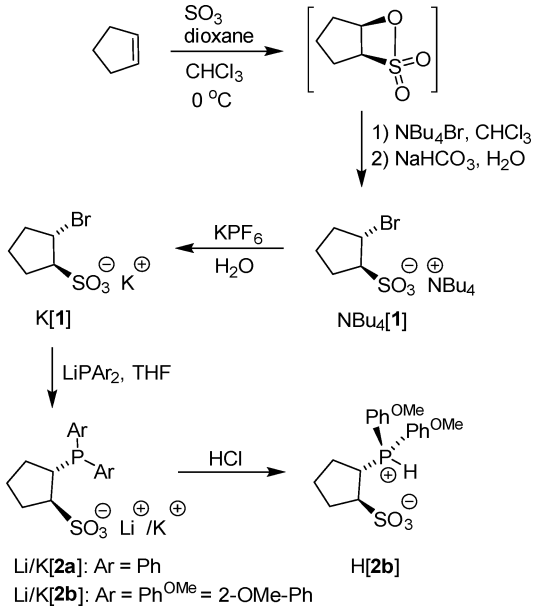

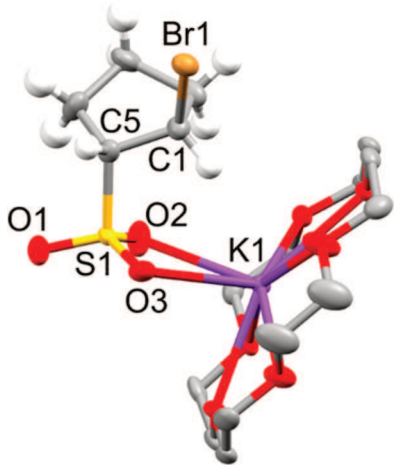

Figure 1. Molecular structure of [K(18-*crown*-6)][**1**]. The H atoms on the 18-*crown*-6 unit are omitted. Selected bond lengths (Å): Br1−C1 1.972(4), S1−C5 1.820(4), S1−O1 1.444(3), S1−O2 1.446(3), S1−O3 1.447(3), K1−O2 2.782(3), K1−O3 2.902(3).

neighboring sulfonate group.[42] Li/K[**2b**] was converted to the phosphonium sulfonate zwitterion H[**2b**] by reaction with excess HCl. The ^{31}P NMR spectrum of H[**2b**] comprises a doublet at δ 9.9 with a large $^{1}J_{PH}$ value (446 Hz), which confirms that H[**2b**] exists as a zwitterion. Attempts to prepare 2-PR_2-cyclopentanesulfonate ligands that contain $-P^iPr_2$, $-P(menthyl)_2$, and $-P(2',6'$-dimethoxybiphenyl$)_2$ units by this route were unsuccessful (see the Supporting Information).

(C5-PO)PdMe(py) Complexes. The reaction of Li/K[**2a**] with (COD)PdMeCl, followed by addition of pyridine, affords (**2a**)PdMe(py) (**3a**) in 85% yield (eq 1). The analogous reaction with Li/K[**2b**] gave a mixture of products, from which {[Li(THF)][(**2b**)PdMeCl]}$_2$ was isolated in low yield (eq 3). The reaction of H[**2b**] with (TMEDA)$PdMe_2$ followed by addition of pyridine affords (**2b**)PdMe(py) (**3b**) in 91% yield (eq 3).

Compound **3a** decomposes thermally within 1 h at 40 °C in chlorobenzene-d_5 to Pd^0 and unidentified ligand-derived

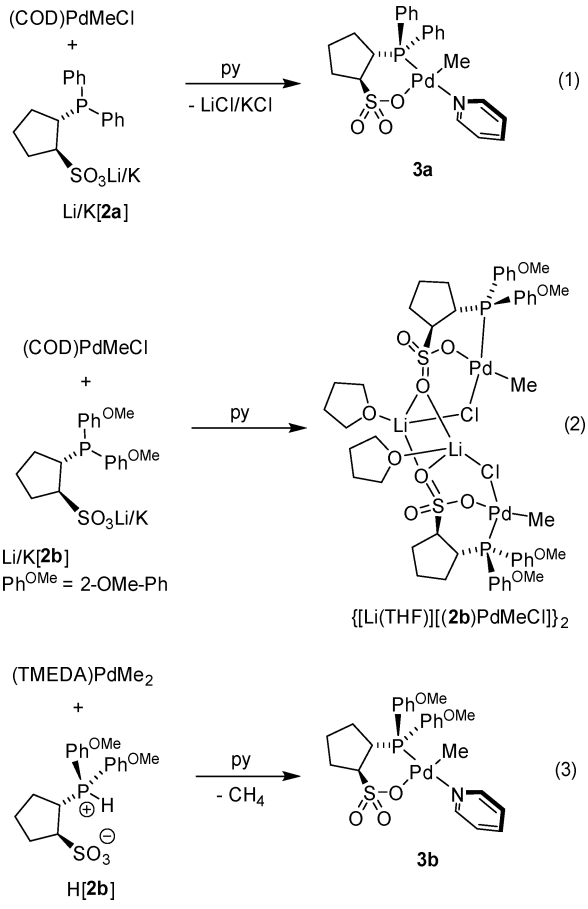

species. In contrast, **3b** is thermally stable in chlorobenzene-d_5 and toluene-d_8 at 80 °C for at least 20 h.

Solid-State Structures of 3a and 3b. The solid-state structures of **3a** and **3b** are shown in Figures 2 and 3 and are very similar to those of the analogous *benzo*-linked complexes (2-PPh_2-benzenesulfonate)PdMe(py) (**3c**)[23] and (2-P(2-OMe-Ph)$_2$-benzenesulfonate)PdMe(py) (**3d**)[43] (Chart 2). Each complex features square-planar geometry at Pd, a six-membered

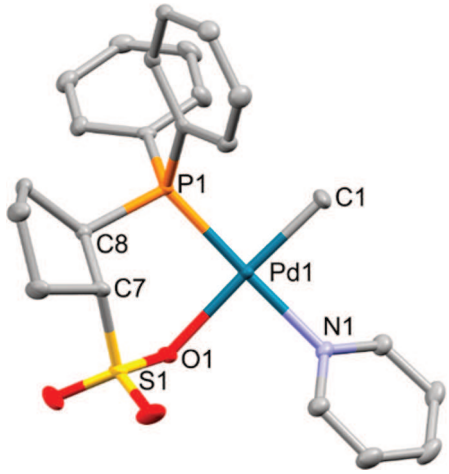

Figure 2. Molecular structure of **3a**. Hydrogen atoms are omitted. Bond lengths (Å) and angles (deg): Pd1−C1 2.020(3), Pd1−N1 2.122(2), Pd1−O1 2.1816(18), Pd1−P1 2.2308(7), C1−Pd1−N1 88.65(10), N1−Pd1−O1 88.64(8), C1−Pd1−P1 89.82(9), O1−Pd1−P1 93.04(5).

DOI: 10.1021/acs.organomet.7b00572
Organometallics 2017, 36, 3415−3428

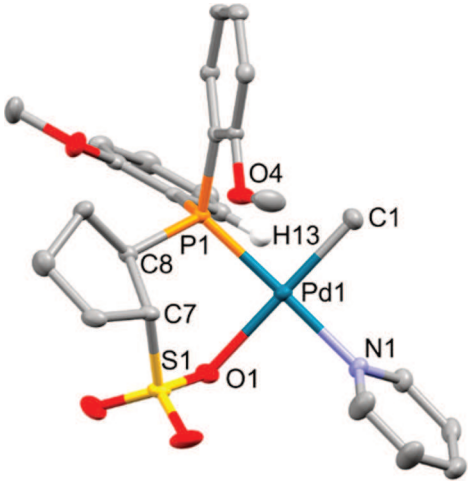

Figure 3. Molecular structure of **3b**·CH_2Cl_2. Hydrogen atoms except H13 and a CH_2Cl_2 solvent molecule are omitted. Bond lengths (Å) and angles (deg): Pd1−C1 2.019(3), Pd1−N1 2.106(2), Pd1−O1 2.195(2), Pd1−P1 2.2324(7), C1−Pd1−N1 91.04(11), N1−Pd1−O1 88.91(8), C1−Pd1−P1 89.96(9), O1−Pd1−P1 90.25(6).

Chart 2. (PAr_2-arenesulfonate)PdRL Complexes

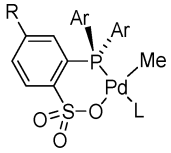

3c, R = H, Ar = Ph, L = py
3d, R = H, Ar = Ph^{OMe}, L = py
3e, R = Me, Ar = Ph^{OMe}, L = py
3f, R = Me, Ar = Ph^{OMe}, L = dmso
3g, R = Me, Ar = 3,5-$^tBu_2$-Ph, L = py

phosphine-sulfonate)Pd chelate ring and a *cis* arrangement of the phosphine and methyl ligands. The Pd−ligand bond distances and the O−Pd−P angles of **3a** and **3b** are nearly identical to those in **3c** and **3d**, respectively.[44] The conformations of the *o*-anisolyl rings in **3b** and **3d** are also similar. In each structure, the −OMe substituent of one *o*-anisolyl ring is directed toward Pd (*exo*) and the −OMe substituent of the other *o*-anisolyl ring is directed away from Pd (*endo*).[18,32,45,46] The *ortho*-H on the *endo* ring (H13 in Figure 3) and the methoxy group on the *exo* ring (O4 in Figure 3) of **3b** are directed toward Pd, but the Pd···H13 (2.799 Å) and Pd···O4 (3.438 Å) distances are close to or greater than the sums of the relevant van der Waals radii (Pd, H: 2.83 Å; Pd, O: 3.18 Å).

The major difference between **3a,b** and their arenesulfonate analogues **3c,d** is that the (PO)Pd chelate rings in **3a,b** are more strongly puckered than those in **3c,d**, as illustrated in Figure 4. One measure of chelate ring puckering is the angle between the O−S−C−C and O−Pd−P planes, which is much larger in **3a** and **3b** (63, 69°) than in **3c** and **3d** (31, 27°).[47]

Solution Structure of 3b. Room-temperature NMR data show that the solution structure of **3b** contains one *exo* and one *endo* *o*-anisolyl ring as observed in the solid-state. The ^1H NMR spectrum of **3b** contains a low-field resonance (δ 8.5) that integrates to 1H, which is characteristic of an *ortho* hydrogen of a P-*aryl* ring that is positioned in the axial, deshielding region of the Pd square plane.[32,48−53] This resonance is assigned to H13

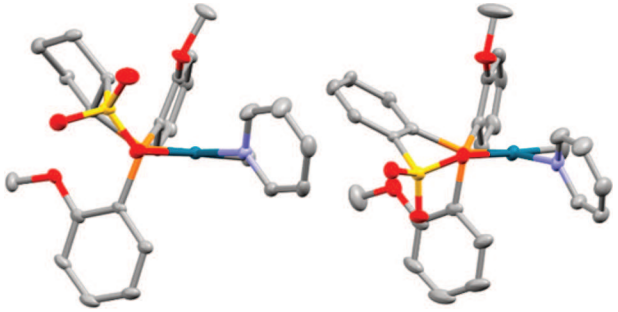

Figure 4. Views of **3b** (left) and **3d**[43] (right) highlighting the puckering of the (PO)Pd chelate rings.

in reference to the numbering scheme in Figure 3. The $^1H-^1H$ NOESY spectrum contains correlations between H13 and the *ortho* hydrogens of the pyridine ligand and the Pd−CH_3 hydrogens, confirming that H13 is directed toward Pd. The *ortho* hydrogen resonance of the other *o*-anisolyl ring appears in the normal range (δ 7.2) and does not have NOESY correlations to the Pd−CH_3 or pyridine resonances, indicating that it is directed away from Pd.

Structure of {[Li(THF)][(2b)PdMeCl]}$_2$. In the solid-state, {[Li(THF)][(**2b**)PdMeCl]}$_2$ adopts a C_2-symmetric structure in which two (**2b**)PdMeCl$^-$ anions are linked by two Li(THF)$^+$ cations (Figure 5). Each Li(THF)$^+$ cation binds one S=*O*

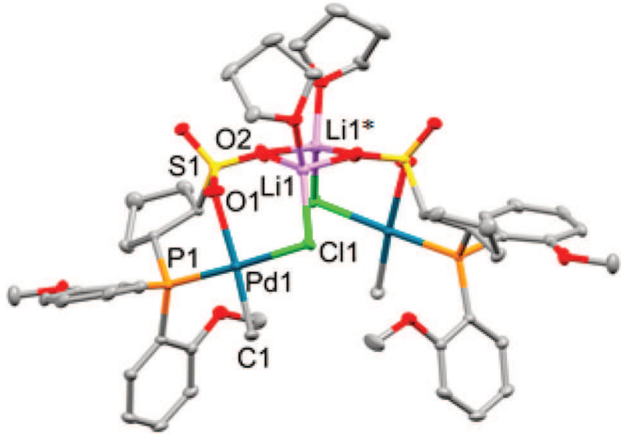

Figure 5. Molecular structure of {[Li(THF)][(**2b**)PdMeCl]}$_2$. Hydrogen atoms are omitted. Selected bond lengths (Å) and angles (deg): Pd1−C1 2.012(2), Pd1−Cl1 2.3898(8), Pd1−O1 2.246(2), Pd1−P1 2.2238(8), Cl1−Li1 2.334(3), O2−Li1 2.094(4), O2−Li1* 1.927(3), C1−Pd1−Cl1 93.09(7), Cl1−Pd1−O1 89.78(5), C1−Pd1−P1 89.17(7), O1−Pd1−P1 88.01(5).

atom of each [(**2b**)PdMeCl]$^-$ unit and one Pd−*Cl* atom to form a 4-membered Li_2O_2 ring and two 6-membered Li−Cl−Pd−O−S−O rings. Several other solvated Li^+-/Na^+-linked dinuclear (PO)Pd(II) complexes are known, and their structures vary depending on the PO$^-$ ligand, alkali metal cation, solvent, and crystallization conditions.[15,24,54−57]

Abstraction of Pyridine from 3b by B(C_6F_5)$_3$ to Generate {(2b)PdMe}$_2$ (4b). The reaction of **3b** with 1 equiv of B(C_6F_5)$_3$ in CH_2Cl_2 produces soluble B(C_6F_5)$_3$(py) and base-free dimer **4b**, which precipitates as a white powder (Scheme 3). Addition of 1 equiv of pyridine or dissolution in a coordinating solvent (Et_2O, THF-d_8, dmso-d_6) converts **4b** to the corresponding (**2b**)PdMe(L) complex. **4b** is insoluble in

DOI: 10.1021/acs.organomet.7b00572
Organometallics 2017, 36, 3415−3428

Scheme 3. Synthesis of 4b and 5b

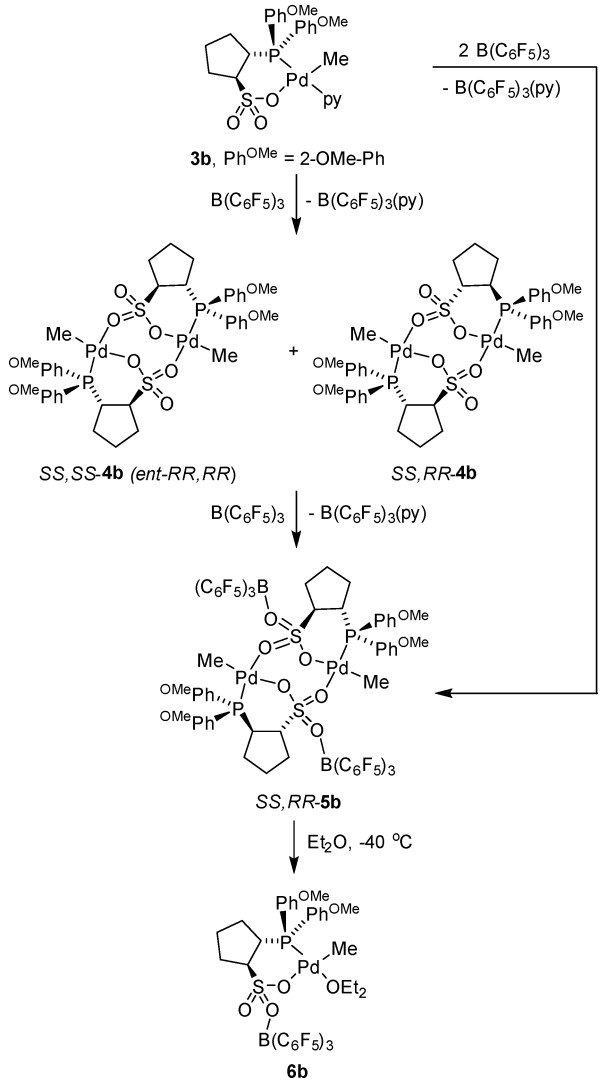

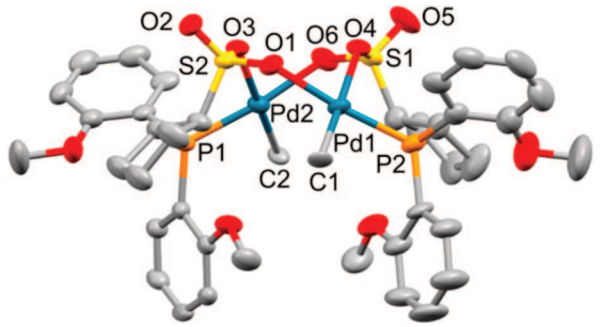

Figure 6. Molecular structure of **4b**·4($CHCl_2CHCl_2$). The *SS,SS*-stereoisomer is shown. Hydrogen atoms and the $CHCl_2CHCl_2$ solvent molecules are omitted. Selected bond lengths (Å) and angles (deg): Pd1−P2 2.208(2), Pd1−O1 2.152(5), Pd1−O4 2.172(5), Pd1−C1 2.060(7), Pd2−P1 2.202(2), Pd2−O3 2.176(5), Pd2−O6 2.152(5), Pd2−C2 2.049(7), O1−Pd1−O4 87.55(19), O4−Pd1−P2 91.98(15), C1−Pd1−P2 89.7(2), C1−Pd1−O1 90.3(3), O3−Pd2−P1 92.51(14), O6−Pd2−O3 87.26(19), C2−Pd2−P1 88.2(2), C2−Pd2−O6 91.8(2).

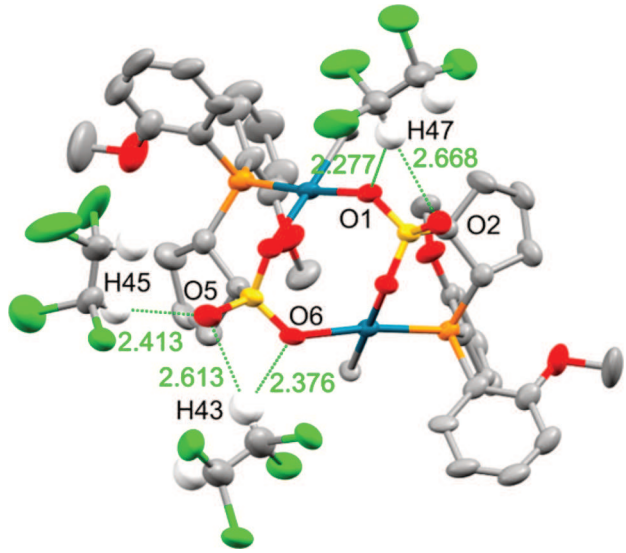

Figure 7. Molecular structure of **4b**·4($CHCl_2CHCl_2$) highlighting the hydrogen bonding interactions involving the $CHCl_2CHCl_2$ solvent molecules and the sulfonate groups of **4b**. The *SS,SS* stereoisomer is shown. The hydrogen atoms of **4b** and the $CHCl_2CHCl_2$ molecule that is not involved in hydrogen bonding are omitted. The disorder in two solvent molecules and the cyclopentane rings is not shown.

CH_2Cl_2, C_6H_5Cl, toluene, and benzene but dissolves in 1,1,2,2-tetrachloroethane-d_2.

Crystals of **4b**·4($CHCl_2CHCl_2$) were grown from a concentrated $CHCl_2CHCl_2$ solution and characterized by X-ray crystallography (Figure 6). Compound **4b** adopts an approximately C_2-symmetric dinuclear structure comprising two *S,S*-(**2b**)PdMe units or two *R,R*-(**2b**)PdMe units that are linked through two sulfonate bridges. The *S,S* and *R,R* stereochemical descriptors denote the configurations of C^1 and C^2 in the cyclopentane ring. The central eight-membered $(PdSO_2)_2$ ring of **4b** adopts a boat−boat conformation,[58,59] in which Pd1 and Pd2 lie on the same side of the plane formed by O1, S2, O3, O6, S1, and O4. The unit cell contains one *SS,SS*-**4b** molecule and one *RR,RR*-**4b** molecule. Interestingly, there are hydrogen bonds between three of the $CHCl_2CHCl_2$ molecules and the sulfonate oxygens in **4b**·4($CHCl_2CHCl_2$) (Figure 7). The CH···O distances are in the range of 2.3−2.7 Å and are shorter than the sum of the H and O van der Waals radii (2.72 Å). These hydrogen bonding interactions provide an explanation for why **4b** is soluble in $CHCl_2CHCl_2$ but not in CH_2Cl_2. CH_2Cl_2 is ca. 2 pK_a units less acidic and is a poorer hydrogen bond donor compared to $CHCl_2CHCl_2$.[60,61]

The structure of **4b** is similar to those of {(*o*-{(2-Et-Ph)$_2$P}-*p*-toluenesulfonate)PdMe}$_2$[36] and {(*o*-{(2-OMe-Ph)$_2$P}-*p*-toluenesulfonate)Pd(CH_2SiMe_3)}$_2$.[62] The main difference is that the central $(PdSO_2)_2$ ring in **4b** adopts a boat−boat conformation, while those in the latter compounds adopt chair−chair conformations.[36,62] {(*o*-{(3,5-^{t}Bu$_2$-Ph)$_2$P}-*p*-toluenesulfonate)PdMe}$_2$ is also known but differs from **4b** in that the (PO-3,5-^{t}Bu$_2$)PdMe units are linked through a four-membered Pd_2O_2 ring.[36]

The ^{1}H NMR spectrum of **4b** in $CDCl_2CDCl_2$ solution contains two Pd−Me resonances in a 3/1 intensity ratio, and the ^{31}P spectrum contains one broad resonance, which is most likely a result of two overlapping signals. The NMR spectra of **4b** are concentration-independent, which implies that **4b** is not in equilibrium with a monomeric (**2b**)PdMe($CDCl_2CDCl_2$) species, since the fraction of the latter species is expected to

DOI: 10.1021/acs.organomet.7b00572
Organometallics 2017, 36, 3415−3428

increase as $[Pd]_{total}$ is decreased, likely resulting in changes to the spectra. Therefore, the two species are assigned as the *SS,SS*-**4b** (*ent-RR,RR*) and *SS,RR*-**4b** diastereomers, which differ in relative configurations of the cyclopentane units in the two halves of the dimer.[63]

Borane-Coordinated Base-Free Dimer 5b. The reaction of **3b** with 2 equiv of $B(C_6F_5)_3$ in CH_2Cl_2 at room temperature yields $B(C_6F_5)_3$(py) and soluble borane adduct $\{$(**2b**·B-$(C_6F_5)_3$)PdMe$\}_2$ (**5b**, Scheme 3). **5b** is also formed by the reaction of **4b** with 2 equiv of $B(C_6F_5)_3$ (i.e., 1 equiv per Pd). Crystallization of **5b** from $CHCl_2CHCl_2$/hexanes in the presence of excess $B(C_6F_5)_3$ affords *SS,RR*-**5b** as colorless crystals. In the solid-state, *SS,RR*-**5b** adopts an S_2-symmetric dinuclear structure consisting of two (**2b**·$B(C_6F_5)_3$)PdMe units linked by two sulfonate bridges (Figure 8). The central eight-membered ring adopts a chair−chair conformation, and the two $B(C_6F_5)_3$ units are located on opposite sides of the central ring.

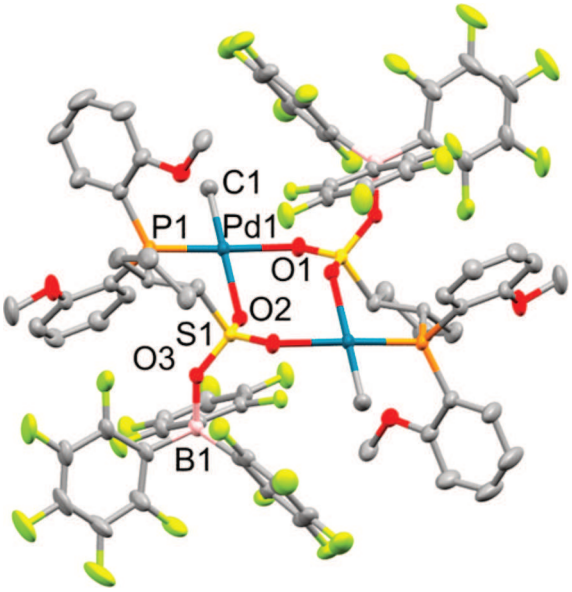

Figure 8. Molecular structure of **5b**·($CHCl_2CHCl_2$). Hydrogen atoms and the $CHCl_2CHCl_2$ solvent molecule are omitted. Selected bond lengths (Å) and angles (deg): Pd1−P1 2.208(2), Pd1−O1 2.2101(19), Pd1−O2 2.204(2), Pd1−C1 2.024(3), S1−O1 1.450(2), O2−S1 1.450(2), S1−O3 1.507(2), O3−B1 1.584(5), O1−Pd1−O2 86.67(7), O2−Pd1−P1 93.56(5), C1−Pd1−P1 88.91(10), C1−Pd1−O1 91.17(11).

The ^{1}H NMR spectrum of **5b** contains several Pd−Me resonances, indicating the presence of several species, which may include stereoisomers and complexes that contain either one or two $B(C_6F_5)_3$ molecules. However, dissolution of **5b** in Et_2O cleanly generates $\{$**2b**·$B(C_6F_5)_3\}$PdMe(Et_2O) (**6b**), which crystallizes at −40 °C as the **6b**·Et_2O solvate (Scheme 3). The ^{1}H NMR spectrum of **6b**·Et_2O at −60 °C in CD_2Cl_2 solution contains separate resonances for free and bound Et_2O (1:1 integral ratio), indicating that only 1 equiv of Et_2O is coordinated. However, exchange of free and **6b**-coordinated Et_2O is fast on the NMR time scale at room temperature, and under these conditions, one set of exchange-averaged Et_2O resonances is observed. Attempts to remove the excess Et_2O from **6b**·Et_2O resulted in significant decomposition of the complex.

Ethylene Polymerization Studies. Ethylene polymerization results are summarized in Table 1.[64] Compound **3b** produces PE with a M_n of ca. 4000 Da with an activity of 100 kg mol^{-1} h^{-1} at 250 psi ethylene and 80 °C in toluene (entry 1). Base-free dimer **4b** is ca. twice as active as **3b** and produces PE with similar MW as **3b**, consistent with both complexes forming the same active (**2b**)PdMe(ethylene) species, entry 2. The 2-fold increase in activity is a result of removing the off-cycle equilibrium between active (**2b**)PdR(ethylene) and inactive (**2b**)PdR(py) species (R = growing chain).[36,62,65,66] $\{$(PO)PdR$\}_2$ catalysts that contain phosphine-arenesulfonate ligands show similar enhancements in activity compared to the corresponding (PO)PdR(py)complexes.[6,8,36,62] The observed activity of **4b** is very similar for 1 and 2 h polymerization reactions, indicating that the catalyst is quite stable under these conditions (entries 2 and 4). Increasing the ethylene pressure to 800 psi has little effect on the catalyst activity or the MW of the resulting PE, suggesting that the rate-determining step is insertion of the (PO)PdR(ethylene) catalyst resting state (entries 2 and 5) and that chain transfer occurs by an associative mechanism.[67] Borane adduct **5b** is less active and produces PE with a 2-fold lower MW compared to **3b** and **4b** (entries 6 and 7). In contrast, binding of $B(C_6F_5)_3$ to (PAr_2-arenesulfonate)PdR catalysts increases activity but results in larger reductions in MW.[36] The T_m values of the PEs produced by **3b**, **4b**, and **5b** (~131 °C) are consistent with highly linear PEs in the observed MW range.[68−70] These PEs contain a mixture of terminal RCH=CH_2 (56−93%) and internal RCH=CHR (7−44%) olefins, and the ratio of unsaturated RCH=CH_2 to saturated RCH_2CH_3 chain ends is ca. 1/1. The observation of ethylene polymerization and a long catalyst lifetime for **4b** contrasts with the ethylene oligomerization and short catalyst lifetime reported for the ethylene-linked analogue **C** (Chart 1).[29] This difference is ascribed to the stabilizing effect of rigidifying the phosphine-alkanesulfonate ligand by the

Table 1. Ethylene Polymerization by 3b, 4b, 5b, and 3e

entry[c]	complex	Pd loading (μmol)	$P_{ethylene}$ (psi)	time (h)	activity (kg mol$_{Pd}^{-1}$ h^{-1})	M_n (Da)[d]	PDI[d]	T_m (°C)[e]
1[a]	**3b**	0.88	250	2	100	4480	1.9	131.8
2[a]	**4b**	0.88	250	2	210	4210	2.0	131.8
3[a]	**4b**	1.6	250	2	190	3610	1.8	131.2
4[a]	**4b**	0.88	250	1	190	5200	2.0	131.3
5[a]	**4b**	0.88	800	2	170	5250	1.6	131.4
6[a]	**5b**	0.88	250	2	34	2050	3.5	129.2
7[b,f]	**3b** + 2 $B(C_6F_5)_3$	0.88	250	2	84	1950	2.2	128.8
8[b]	**3e**	0.88	250	2	1330	16400	1.9	135.2

[a]Noninjection protocol, 50 mL of toluene, 80 °C. [b]Injection protocol, 40 mL of toluene, 10 mL of chlorobenzene catalyst solution, 80 °C. [c]Average of at least two runs. [d]Determined by GPC. [e]Determined by DSC. [f]*In situ* generation of **5b** from **3** + 2$B(C_6F_5)_3$.

DOI: 10.1021/acs.organomet.7b00572
Organometallics 2017, 36, 3415−3428

incorporation of the cyclopentane linker in **4b**. However, **3b**, **4b**, and **5b** are much less active and produce PE with lower MWs compared to phosphine-arenesulfonate analogue **3e** (entry 8, Table 1).

Copolymerization of Ethylene with Methyl Acrylate by 3b and 4b. The results of ethylene/MA copolymerization by **3b** and **4b** (eq 4) are summarized in Table 2. At 400 psi

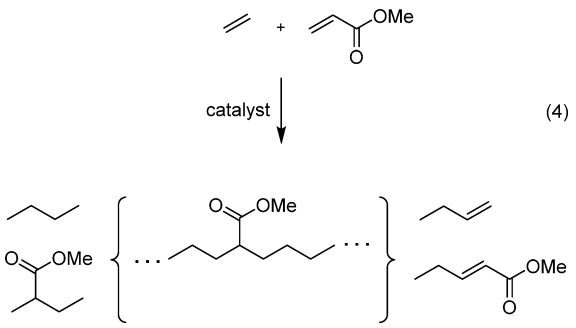

ethylene, 1.2 M MA and 80 °C, **3b** and **4b** produce copolymers with low MWs and 3.3−3.8 mol % MA incorporation (entries 1 and 2). Increasing the $[MA]/P_{ethylene}$ ratio results in an increase in MA incorporation as expected (Figure 9).[6,17,18,24] Under otherwise identical conditions, increasing the concentration of MA from 0.7 to 1.2 M increases the MA incorporation from 1.8 to 3.3 mol %, lowers the catalyst activity, and slightly decreases the copolymer MW (entries 2 and 3). Increasing the amount of MA in the copolymer significantly decreases the T_m value.

3b and **4b** incorporate MA mainly as $-CH_2CH(CO_2Me)CH_2-$ in-chain units (80%), with lower amounts of $-CH_2CH(CO_2Me)Me$ (8%) and $-CH{=}CHCO_2Me$ (12%) chain-end units observed (eq 4). These results imply that chain growth is favored over chain transfer following a MA insertion. The sum of saturated end groups is roughly equal to the sum of unsaturated end groups (see Table S4).

Interestingly, while **4b** is only ca. 2 times as active as **3b** in ethylene homopolymerization, it is ca. 6 times more active than **3b** in ethylene/MA copolymerization. A possible explanation for this difference is that pyridine competes more strongly with ethylene for coordination to Pd after a MA insertion than after an ethylene insertion, i.e., the K_{eq} value for eq 6 is greater than that for eq 5.

4b is less active in ethylene/MA copolymerization and produces copolymer with a lower MW, but incorporates a similar amount of MA (entries 4−7, Table 2), compared to the arenesulfonate analogues **3e**[71] and **3f**[6] (Chart 2). Compounds

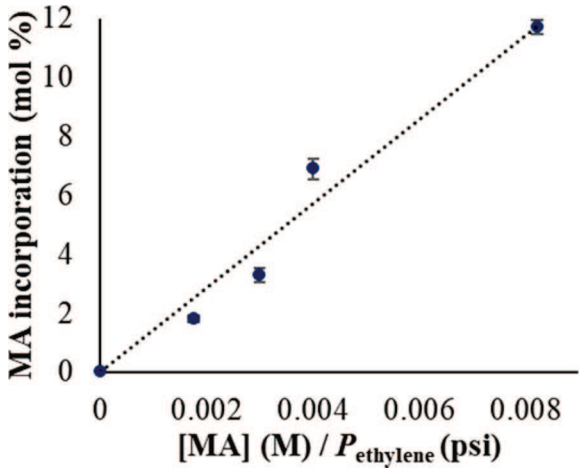

Figure 9. Dependence of MA incorporation on monomer feed ratio in ethylene/MA copolymerization by **4b** at 80−100 °C in toluene or toluene/chlorobenzene.

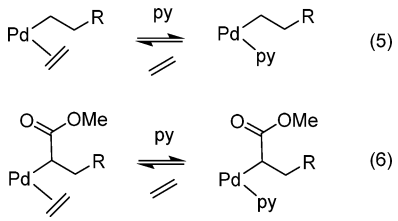

3b and **3e** are both an order of magnitude less active in ethylene/MA copolymerization than in ethylene homopolymerization and produce copolymers with half the M_n value of their respective PEs, indicating that these cyclopentane and arene-linked (PO)PdR complexes suffer from a similar degree of inhibition in the presence of MA.

Copolymerization of Ethylene and Vinyl Fluoride by 3b and 4b. The results of ethylene/VF copolymerization by **3b** and **4b** are summarized in Table 3. At 80 °C, 220 psi ethylene, and 80 psi VF, **3b** and **4b** incorporate ca. 0.1 mol % VF (entries 1−3). Under these conditions, the activity of each complex is severely depressed and the M_n value of the copolymer produced is similar relative to what is observed in ethylene homopolymerization. Increasing the VF pressure to 160 psi increases the VF incorporation level to 0.4 mol % and decreases the copolymer M_n by half, but it does not strongly influence the activity (entry 4).

Table 2. Copolymerization of Ethylene and Methyl Acrylate (MA) by 3b, 3e, 3f, and 4b

entry[h]	complex	Pd loading (μmol)	$P_{ethylene}$ (psi)	[MA] (M)	activity (kg mol_{Pd}^{-1} h^{-1})	M_n (Da)[e]	PDI[e]	MA incorp (mol %)[f]	T_m (°C)[g]
1[a]	**3b**	15	400	1.2	4.0	2230	2.0	3.8	110.5
2[b]	**4b**	15	400	1.2	23	2130	2.3	3.3	112.8
3[b]	**4b**	15	400	0.7	30	2520	2.6	1.8	121.7
4[c]	**4b**	13	300	1.2	15	1750	1.7	6.9	94.7
5[c]	**3e**	13	300	1.2	107	9800		6.3	
6[d]	**4b**	20	73	0.6	5.0	1830	1.5	11.7	68.2
7[d]	**3f**	20	73	0.6	130	2500	2.3	9.4	

[a]Conditions: injection procedure, 34.6 mL of toluene, 10 mL of chlorobenzene, 5.44 mL of MA, and 0.1 g of BHT, 80 °C, 2 h. [b]Conditions: noninjection procedure, 34.6 mL of toluene, 10 mL of chlorobenzene, 5.44 mL of MA, 0.1 g of BHT, 80 °C, 2 h. [c]Conditions:[71] 44.7 mL of toluene, 5.3 mL of MA, 1 mg of BHT, 100 °C, 1 h. [d]Conditions:[6] 47.3 mL of toluene, 2.7 mL of MA, 1 mg of BHT, 95 °C, 1 h. [e]Determined by GPC. [f]Determined by ^{1}H NMR; in all cases MA incorporated as $-CH_2CH(CO_2Me)CH_2-$ (80%), $-CH_2CH(CO_2Me)Me$ (8%), and $-CH_2CH{=}CH(CO_2Me)$ (12%)units. [g]Determined by DSC. [h]Average of two runs.

DOI: 10.1021/acs.organomet.7b00572
Organometallics 2017, 36, 3415−3428

Table 3. Copolymerization of Ethylene and Vinyl Fluoride (VF) with 3b, 4b, and 3e

entry	complex	[Pd] (μmol)	E (psi)	VF (psi)	activity (kg mol_{Pd}^{-1} h^{-1})	M_n (Da)[c]	PDI[c]	VF incorp (mol %)[d]	T_m (°C)[e]
1[a]	**3b**	0.88	220	80	5.7	4360[d]	n.d.	0.1	n.d.
2[a]	**3b**	8.8	220	80	2.6	4540	2.9	0.1	130.0
3[b,f]	**4b**	20	220	80	17	4180	1.6	0.1	131.1
4[b,f]	**4b**	20	220	160	15	1950	2.0	0.4	125.5
5[b]	**3e**	10	220	80	4.5	8100	1.9	0.5	n.d.

[a]Conditions: injection procedure, 40 mL of toluene, 10 mL of chlorobenzene, 80 °C, 2 h. [b]Conditions: noninjection procedure, 50 mL of toluene, 80 °C, 2 h. [c]Determined by GPC. [d]Determined by ^{1}H NMR. [e]Determined by DSC. [f]Average of two runs.

The microstructures of the ethylene/VF copolymers produced by **3b** and **4b** are summarized in Table 4.

Table 4. Microstructures of E/VF Copolymers Produced by 3b, 4b, and 3e[19]

	VF incorporation mode (%)[a]			
catalyst	$-CH_2CF_2H$	$-CH_2CH_2F$	$-CH_2CHFCH_2-$	$-CH_2CHFCH_3$
3b[b]	12	7	77	4
4b[b]	10	1	81	7
4b[c]	7	8	80	5
3e[b]	13	8	76	2

[a]Determined by ^{19}F NMR; values determined by ^{1}H NMR are similar. [b]Copolymerization in 4/1 toluene/chlorobenzene, 220 psi ethylene, 80 psi VF. [c]Copolymerization in 4/1 toluene/chlorobenzene, 220 psi ethylene, 160 psi VF.

Approximately 80% of the VF is present as internal $-CH_2CHFCH_2-$ units, which arise from 1,2- or 2,1-insertion of VF into a growing (PO)PdR species followed by ethylene insertion. Three chain-end units are also observed: (i) $-CH_2CF_2H$, formed by 1,2-insertion of VF into a (PO)PdF species (generated by β-F elimination) followed by ethylene insertion, (ii) $-CH_2CHFCH_3$, formed by 2,1-insertion of VF into a (PO)PdH species followed by ethylene insertion, and (iii) $-CH_2CH_2F$, formed by insertion of ethylene into a (PO)PdF species or 1,2-insertion of VF into a (PO)PdH species followed by ethylene insertion.[10,19] Unsaturated $-CH_2CH{=}CHF$ chain-end units, which can form by 2,1-VF insertion into a (PO)PdR species followed by β-H transfer, were not observed.[72]

3b and **4b** display similar activity for ethylene/VF copolymerization compared to that of phosphine-arenesulfonate complex **3e** but produce copolymers with lower MWs and less VF incorporation (entry 5, Table 3). The microstructures of the E/VF copolymers produced by **3b**, **4b**, and **3e** are also similar (Table 4).[19]

Ethylene Insertion of (2b)PdMe(C_2H_4). As noted above, the observation that the activity of **4b** is independent of ethylene pressure (over the range 250−800 psi) suggests that the catalyst resting state is the ethylene adduct (**2b**)PdR(ethylene). Low-temperature NMR studies were pursued to probe the properties and ethylene insertion of such species. The reaction of base-free dimer **4b** with excess ethylene (12 equiv vs Pd) at low temperature (below 0 °C) results in quantitative formation of (**2b**)PdMe(ethylene) (**7b**, Scheme 4). The ^{31}P NMR resonance of **7b** (δ 36.2), which contains a soft ethylene ligand *trans* to the phosphine, is shifted upfield by 10−15 ppm from those of **3b** (δ 46.3), **4b** (δ 50.9), **5b** (δ 51.1), and **6b** (δ 49.9), which contain hard nitrogen or oxygen ligands *trans* to the phosphine. A similar chemical shift difference was observed among {*o*-P(3,5-^{t}Bu$_2$-Ph)$_2$-*p*-toluenesulfonate}PdMe(ethylene) (δ 15.9), {*o*-P(3,5-^{t}Bu$_2$-Ph)$_2$-*p*-toluenesulfonate}PdMe(py) (δ 30.5), and [{*o*-P(3,5-^{t}Bu$_2$-Ph)$_2$-*p*-toluenesulfonate}PdMe]$_2$ (δ 33.0).[36] The ^{13}C{^{1}H} NMR spectrum of **7b** contains a singlet at δ 1.02 for the Pd−*Me* group. The absence of observable ^{31}P−^{13}C coupling establishes that the Me ligand is *cis* to the phosphine. Exchange of free and coordinated ethylene is fast on the NMR time scale for **7b** even at −35 °C, and one exchange-averaged ethylene signal is observed in the ^{1}H and ^{13}C NMR spectra.[73] A correlation between the Pd−CH_3 resonance and the exchange-averaged ethylene resonance is present in the ^{1}H−^{1}H NOESY spectrum, which provides conclusive evidence that **7b** contains an ethylene ligand.

Scheme 4. Reaction of 4b with Ethylene

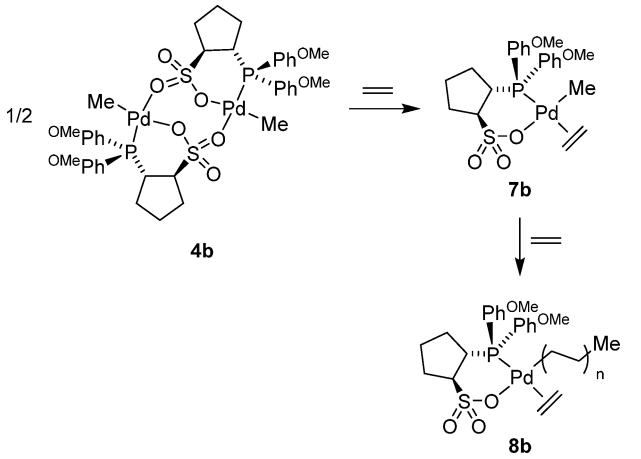

Complex **7b** undergoes multiple ethylene insertions at 5 °C to generate a mixture of (**2b**)Pd{$(CH_2CH_2)_n$Me}(ethylene) higher-alkyl species. The ^{1}H NMR resonances for the **2b**$^-$ ligand do not change significantly as chain growth proceeds, but broad peaks in the δ 1.3−0.4 region grow in due to the Pd-alkyl chains. These alkyl resonances are similar to those observed for {P(2-OMe-Ph)$_2$-benzenesulfonate}Pd(CH_2CH_2R)(2,6-lutidine) species with long alkyl chains.[34,36] After 65 min, ca. 9 equiv of ethylene was consumed, and a white precipitate (PE or long-chain (**2b**)Pd(CH_2CH_2R)(ethylene) species) was present.

In a previous study of polyethylene chain growth by {*o*-P(3,5-^{t}Bu$_2$-Ph)$_2$-*p*-toluenesulfonate}PdMe(ethylene), the rate constant for ethylene insertion was determined by tracking the disappearance of the Pd*Me* resonance by ^{1}H NMR.[36] This approach is not possible for **7b**, because chain growth is accompanied by the growth of a resonance (δ 0.09) in the same region as the Pd*Me* resonance of **7b** (δ 0.07). Therefore, an apparent rate constant $k_{insert,PdR(ethylene)}$, which is a composite rate constant for insertion of all (**2b**)PdR(ethylene) species (R = Me, CH_2CH_2R, H) was determined by monitoring the disappearance of the ethylene resonance. Ethylene consump-

DOI: 10.1021/acs.organomet.7b00572
Organometallics 2017, 36, 3415−3428

tion was found to be zero-order in ethylene (Figure 10), consistent with the rate law in eq 7,

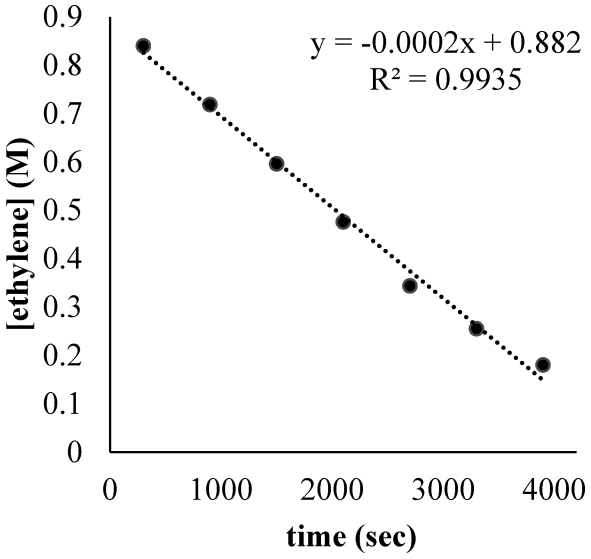

Figure 10. Plot of [ethylene] versus time for the reaction of (**2b**)PdMe(C_2H_4) (**7b**) with ethylene at 5 °C in $CDCl_2CDCl_2$ solvent.

$$\frac{-\mathrm{d[ethylene]}}{\mathrm{d}t} = k_{\mathrm{insert,PdR(ethylene)}}[\mathrm{Pd}] \quad (7)$$

where $k_{\mathrm{insert,PdR(ethylene)}} = 3.0 \times 10^{-3}$ s^{-1} (5 °C, [Pd] = 0.067 M). The corresponding insertion barrier, $\Delta G^{\ddagger}_{\mathrm{insert}}$ = 19.5 kcal/mol, agrees well with the value estimated from the apparent polymerization activity (20 kcal/mol).[74]

DFT Analysis of Ethylene Insertion of 7b and Comparison with Arene-Linked Analogues. As noted above, **3b** and **4b** are approximately an order of magnitude less active than phosphine-arenesulfonate analogue **3e**. DFT computations (B3LYP/6-31G* and Lan12dz) for the rate-limiting ethylene insertion of the corresponding (PO)Pd(R)-(ethylene) species were carried out to probe the origin of this difference.

The ethylene polymerization mechanism by arene-linked (PO)PdMeL complexes has been thoroughly explored by DFT by Ziegler and co-workers[75,76] and Nozaki, Morokuma, and co-workers.[34,67,77] Their results show that *cis-P,R*-(PO)Pd(R)-(ethylene) species are more stable than the corresponding *trans-P,R* isomers and that the lowest-barrier insertion pathway comprises isomerization of the *cis-P,R* isomer to the *trans-P,R* isomer followed by migratory insertion, rather than direct insertion of the *cis-P,R* isomer. Nozaki, Morokuma, and co-workers found that the *cis-P,R*/*trans-P,R* isomerization proceeds via a five-coordinate transition state in which the sulfonate group is bound in a κ^2 fashion.[34,35,78,79]

The model system (2-PMe_2-cyclopentanesulfonate)Pd(Pr)-(ethylene) (**8-C5-PMe_2-Pr**, Chart 3) was first examined to enable comparison with earlier results for the (2-PMe_2-benzenesulfonate)Pd(Pr)(ethylene) (**8-benzene-PMe_2-Pr**) system.[34] The processes examined include the isomerization of *cis-P,C*-isomers **8** to *trans-P,C*-isomers **8′** and the insertion of each of these species. The results are also shown in Figure 11, in which the free energies (*G*, kcal/mol) at 353 K are expressed relative to complexes **8-C5-PMe_2-Pr** and **8-benzene-PMe_2-Pr**. Consistent with earlier findings, in both model complexes, the

Chart 3. Model Compounds Studied by DFT

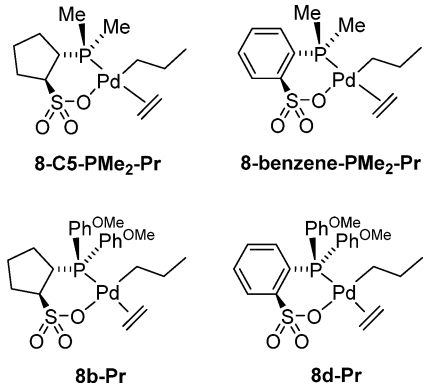

cis-P,R isomers are more stable than the *trans-P,R* isomers, and the lowest-barrier insertion pathway involves *cis*/*trans* isomerization followed by migratory insertion of the *trans-P,R* isomer. Interestingly, the *cis*/*trans* isomerization is less endergonic and has a lower barrier for **8-C5-PMe_2-Pr** than for **8-benzene-PMe_2-Pr**, but the barrier to insertion of the *trans-P,R* isomer is slightly higher in the former case. These results show that the chain growth rate is controlled by the barrier to insertion of the *trans-P,R* isomer in both systems. Accordingly, this barrier was calculated for {2-P(2-OMe-Ph)$_2$-cyclopentanesulfonate)Pd-(Pr)(ethylene) (**8b-Pr**, Chart 3) and the benzene-linked analogue **8d-Pr**. As shown in Figure 11, the barrier for insertion of the *trans-P,R* isomer is 1.6 kcal/mol higher for **8b-Pr** than for **8d-Pr**. This result implies that the lower ethylene polymerization activity of **3b** and **4b** compared to analogous (phosphine-arenesulfonate)PdR catalysts is due to a slower ethylene insertion rate. However, due to the similary of the insertion barriers, it is not possible to identify the structural/electronic origin of this difference.

CONCLUSION

The Pd(II) alkyl complex {P(2-OMe-Ph)$_2$-cyclopentanesulfonate}PdMe(pyridine) (**3b**) and the corresponding base-free dimer [{P(2-OMe-Ph)$_2$-cyclopentanesulfonate}PdMe]$_2$ (**4b**) polymerize ethylene to linear PE and copolymerize ethylene with MA and VF to linear copolymers. The ethylene polymerization activity is independent of ethylene pressure over the range 250−800 psi. **4b** reacts with ethylene at low temperature to form ethylene adduct *cis-P,R*-{*P*(2-OMe-Ph)$_2$-cyclopentanesulfonate}PdMe(ethylene) (**7b**), which undergoes insertion at 5 °C. These results show that ethylene polymerization by **4b** proceeds by rate-limiting insertion of {P(2-OMe-Ph)$_2$-cyclopentanesulfonate}PdR-(ethylene) species. **3b** and **4b** are much more active and robust than the analogous {P(2-OMe-Ph)$_2$$CH_2CH_2SO_3$)PdR catalyst, which is ascribed to the enhanced molecular rigidity imparted by the cyclopentane linker. However, **3b** and **4b** are less active and produce PE with lower MWs compared to analogous phosphine-arenesulfonate catalysts. DFT calculations show that this difference in activity results from a higher ethylene insertion barrier for the {P(2-OMe-Ph)$_2$-cyclopentanesulfonate}PdR system.

EXPERIMENTAL SECTION

General Procedures. All experiments were performed using drybox or Schlenk techniques under a nitrogen atmosphere unless noted otherwise. Nitrogen was purified by passage through Q-5

DOI: 10.1021/acs.organomet.7b00572
Organometallics 2017, 36, 3415−3428

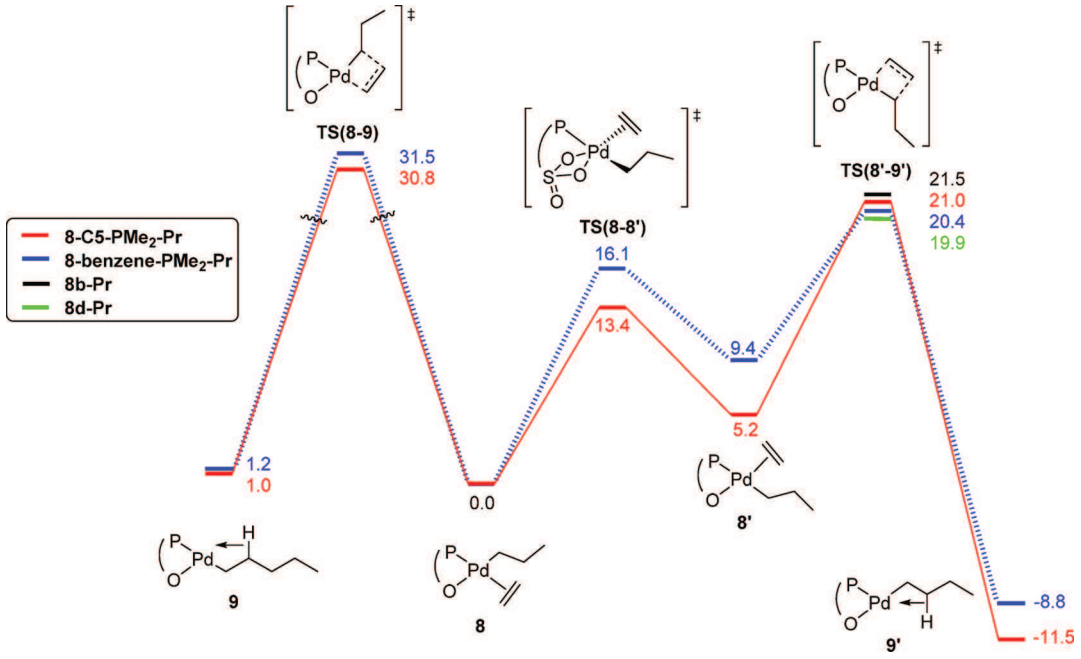

Figure 11. Computed free energy profile for chain growth of model complexes **8-C5-PMe$_2$-Pr** (red) and **8-benzene-PMe$_2$-Pr** (blue), and complexes **8b-Pr** (black) and **8d-Pr** (green). Free energies evaluated at 353 K are given in kcal/mol relative to those for starting complexes **8**. Starting at complex **8**, the direct insertion pathway is shown on the left and the indirect isomerization/insertion pathway is shown on the right.

oxygen scavenger and activated molecular sieves. CH_2Cl_2, Et_2O, and THF were dried by passage through activated alumina. Pentane, hexanes, and toluene were purified by passage through BASF R3−11 oxygen scavenger and activated alumina. CD_2Cl_2 was distilled from and stored over P_2O_5. Toluene-d_8 and THF-d_8 were distilled from Na/benzophenone. DMSO-d_6, cyclopentene, sulfur trioxide (stored in a 35 °C oil bath to prevent formation of fibrous β-SO_3),[80] $CHCl_3$ (50 ppm hexanes as preservative), dioxane (anhydrous), NBu_4Br, KPF_6, $HPPh_2$, ^{n}BuLi solution (1.6 or 2.5 M in hexanes), 2-bromoanisole, diethylphosphite, $HSiCl_3$, NEt_3 (99.5%), ethanol (anhydrous), acetonitrile (anhydrous, 99.8%), $NaHCO_3$, KOH, HCl solution (2.0 M in Et_2O), pyridine (Fisher), 2,6-lutidine (99+%), and 3-phenylpyridine were purchased from Sigma-Aldrich and used without further purification. $B(C_6F_5)_3$ was donated by Boulder Scientific. Ethylene (polymer-grade) and vinyl fluoride (VF) were purchased from Matheson. LiP(2-OMe-Ph)$_2$,[38−41] (COD)PdMeCl (COD = cyclooctadiene),[81] and (TMEDA)PdMe$_2$ (TMEDA = tetramethylethylene diamine)[82] were prepared according to the literature.

NMR spectra were recorded on Bruker DMX-500 or DRX-400 spectrometers at ambient temperature unless otherwise indicated. ^{1}H and ^{13}C chemical shifts are reported relative to $SiMe_4$ and internally referenced to residual ^{1}H and ^{13}C solvent resonances. ^{31}P chemical shifts are externally referenced to 85% H_3PO_4 (δ 0.0). ^{11}B and ^{19}F chemical shifts are externally referenced to $BF_3(OEt_2)$ (δ 0.0 for ^{11}B and δ −153 for ^{19}F).

Electrospray mass spectra (ESI-MS) and atmospheric pressure chemical ionization mass spectra (APCI-MS) were recorded using Agilent 6224 TOF−MS (high-resolution) or 6130 LCMS (low-resolution) instruments. The observed isotope patterns closely matched calculated isotope patterns. The listed m/z value corresponds to the most intense peak in the isotope pattern.

(2a)PdMe(py) (3a). Li/K[**2a**] (0.1925 g, 0.5170 mmol) and (COD)PdMeCl (0.140 g, 0.509 mmol) were dissolved in CH_2Cl_2 (20 mL), and the mixture was stirred at room temperature for 1.5 h. Pyridine (41 μL, 0.51 mmol) was added and the mixture was stirred at room temperature for 30 min. The mixture was filtered through a fine porosity frit and concentrated under vacuum to 4 mL. Pentane (40 mL) was added to precipitate the product as a white solid. The product was collected by filtration and dried under vacuum (0.22 g, 85%). The numbering scheme for **3a** is shown in Figure 12. ^{1}H NMR

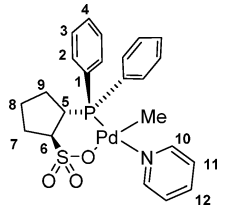

Figure 12. Numbering scheme for **3a**.

(CD_3OD): δ 8.76 (d, $^3J_{HH}$ = 3.5 Hz, 2H, H^{10}), 8.10 (t, $^3J_{HH}$ = 9 Hz, 2H, H^4), 8.02 (t, $^3J_{HH}$ = 7.5 Hz, 1H, H^{12}), 7.72 (t, $^3J_{HH}$ = 8.5 Hz, 2H, H^2), 7.65 (t, $^3J_{HH}$ = 6.5 Hz, 2H, H^{11}), 7.59 (br m, 6H, 4-H^3, 2-H^2), 3.50−3.60 (m, 1H, H^6), 3.20−3.30 (m, 1H, H^5), 2.00−2.15 (m, 2H, H^7, H^9), 1.82−1.93 (m, 1H, H^9), 1.69−1.80 (m, 1H, H^8), 1.54−1.66 (m, 1H, H^7), 1.30−1.40 (m, 1H, H^8), 0.46 (s, 3H, PdCH_3). ^{13}C NMR (CD_3OD): δ 151.6 (2-C^{10}), 137.5 (C^4), 133.4 (C^2), 132.0 (C^{12}), 130.1 (br, 3C, C^3, 2-C^{11}), 126.6 (C^2), 62.7 (C^5), 41.1 (d, $^2J_{PC}$ = 24 Hz, C^6), 30.3 (C^7), 29.9 (C^9), 26.6 (C^8), 0.3 (PdCH$_3$). ^{31}P{^{1}H} NMR (CD_3OD): δ 39.9. ES-HRMS (m/z): Calcd for $[C_{23}H_{26}NO_3PPdS - py + H]^+$ 455.0063. Found: 455.0063. X-ray quality crystals of **3a** were obtained by crystallization from a solution of **3a** (20 mg) in CD_3OD (0.5 mL) at room temperature.

(2b)PdMe(py) (3b). H[**2b**] (0.3005 g, 0.7610 mmol) and (TMEDA)PdMe$_2$ (0.1925 g, 0.7610 mmol) were dissolved in CH_2Cl_2 (16 mL), and the mixture was stirred at room temperature for 1 h. Pyridine (92 μL, 1.2 mmol) was added, and the mixture was stirred at room temperature for 30 min. The mixture was filtered through a fine porosity frit, and the volatiles were removed under vacuum overnight to yield **3b** as a white solid (0.3297 g, 73%). The numbering scheme for **3b** is shown in Figure 13. ^{1}H NMR (CD_2Cl_2): δ 8.85 (d, $^3J_{HH}$ = 5 Hz, 2H, H^{20}), 8.50 (br s, 1H, H^6), 7.92 (t, $^3J_{HH}$ = 7.5 Hz, 1H, H^{22}), 7.64 (t, $^3J_{HH}$ = 8 Hz, 1H, H^4), 7.52 (m, $^2J_{HH}$ = 7.5 Hz, 3H, H^{10}, H^{21}), 7.17 (br s, H^{12}), 7.16 (t, $^3J_{HH}$ = 7 Hz, 1H, H^5), 7.06 (m, 2H, H^9, H^3), 6.98 (t, $^3J_{HH}$ = 7.5 Hz, 1H, H^9, H^{11}), 4.08 (br m, 1H, H^{14}), 3.99 (s, 3H, H^{18}), 3.82 (s, 3H, H^{19}), 3.23 (br m, 1H, H^{13}), 2.17−2.26 (m, 1H, H^{15}), 2.08−2.17 (m, 1H, H^{17}), 2.01−2.08 (m, 1H, H^{15}), 1.77−1.86 (m, 1H, H^{16}), 1.62−1.77 (m, 2H, H^{17}, H^{16}), 0.17 (d, 3H, $^3J_{PH}$ = 2.5 Hz, PdCH_3). ^{13}C{^{1}H} NMR (CD_2Cl_2): δ 160.5 (C^2), 160.0

DOI: 10.1021/acs.organomet.7b00572
Organometallics 2017, 36, 3415−3428

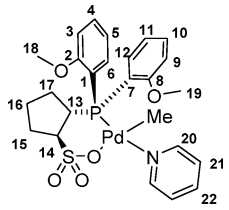

Figure 13. Numbering scheme for **3b**.

(C[8]), 150.6 (C[20]), 139.9 (br s, C[6]), 138.3 (C[22]), 135.5 (br s, C[12]), 133.8 (C[4]), 132.7 (C[10]), 125.0 (C[21]), 120.8 (d, J_{PC} = 14 Hz, C[11]), 120.7 (d, $^3J_{PC}$ = 10 Hz, C[5]), 117.5 (d, $^1J_{PC}$ = 50 Hz, C[1]), 115.2 (d, $^1J_{PC}$ = 50 Hz, C[7]), 110.9 (d, $^3J_{PC}$ = 4 Hz, C[3]), 110.5 (d, $^3J_{PC}$ = 5 Hz, C[9]), 65.7 (d, $^2J_{PC}$ = 9 Hz, C[14]), 55.3 (C[18]), 55.1 (C[19]), 40.9 (d, $^1J_{PC}$ = 32 Hz, C[13]), 30.8 (d, $^2J_{PC}$ = 6 Hz, C[17]), 29.7 (d, $^3J_{PC}$ = 11 Hz, C[15]), 26.0 (d, $^3J_{PC}$ = 7 Hz, C[16]), −1.0 (d, $^2J_{PC}$ = 4 Hz, PdCH$_3$). ^{31}P{^{1}H} NMR (CD_2Cl_2): δ 46.3 (s). ES-HRMS (m/z): Calcd for $[C_{25}H_{30}NO_5PPdS - py + H]^+$ 515.027. Found: 515.026. Crystalline **3b** was obtained by slow diffusion of ether (10 mL) into a solution of **3b** (77 mg) in CH_2Cl_2 (2 mL) at −40 °C. X-ray quality crystals of **4b** were obtained by a second slow diffusion crystallization of this material at −40 °C.

{(2b)PdMe}$_2$ (4b). **3b** (0.250 g, 0.420 mmol) and $B(C_6F_5)_3$ (0.215 g, 0.420 mmol) were dissolved in CH_2Cl_2 (12 mL), and the mixture was stirred in an aluminum foil-coated vial at room temperature for 30 min. The mixture was left to stand overnight resulting in the precipitation of a white solid. The precipitate was collected by filtration, washed with CH_2Cl_2, and dried under vacuum to yield **4b** as a white powder (0.135 g, 62%). NMR studies show that **4b** exists as a 3/1 mixture of two Pd-Me species in $CDCl_2CDCl_2$ solution. ^{1}H NMR ($CDCl_2CDCl_2$): 8.52 (ArH), 7.61 (ArH), 7.45 (ArH), 7.20 (ArH), 7.00 (ArH), 6.85 (ArH), 6.65 (ArH), 4.49 (C5-ring CH), 3.98 (9.3H, −OCH$_3$), 3.89 (4.1H, −OCH$_3$), 3.72 (13.2H, −OCH$_3$), 3.04 (C5-ring CH), 2.28 (C5-ring CH$_2$), 2.09 (C5-ring CH$_2$), 1.74 (C5-ring CH$_2$), 1.64 (C5-ring CH$_2$), 0.39 (s, 3H, Pd−Me), 0.27 (s, 9.8H, PdCH$_3$). ^{31}P NMR ($CDCl_2CDCl_2$): δ 50.8 (br). CI/ESI-HRMS (m/z): Calcd for $[C_{40}H_{50}O_{10}P_2Pd_2S_2 + H]^+$: 1029.0463. Found: 1029.0471. X-ray quality crystals of **4b** were obtained from a concentrated solution of **4b** in $CHCl_2CHCl_2$ in a sealed tube at room temperature.

{(2b·B(C$_6$F$_5$)$_3$)PdMe}$_2$ (5b). *From 3b.* **3b** (0.20 g, 0.34 mmol) and $B(C_6F_5)_3$ (0.35 g, 0.67 mmol) were dissolved in CH_2Cl_2 (12 mL), and the mixture was stirred at room temperature for 2 h. The mixture was concentrated to 4 mL under vacuum, filtered through a syringe filter, and layered with hexanes (12 mL). After 7 days at room temperature, pale yellow crystals formed. The crystalline solid was collected by filtration, washed with hexanes, and dried under vacuum overnight to remove all methylene chloride (220 mg, 32%). X-ray quality crystals of **5b** were obtained from a solution of this crystalline material and excess $B(C_6F_5)_3$ (ca. 2 equiv) in $CHCl_2CHCl_2$ (3 mL) that was layered with hexanes (15 mL) and stored at room temperature. ^{1}H NMR ($CDCl_2CDCl_2$): 8.21 (ArH), 7.64 (ArH), 7.46 (ArH), 7.05 (ArH), 6.88 (ArH), 6.84 (ArH), 6.37 (ArH), 4.49 (C5-ring CH), 4.00 (−OCH$_3$), 3.75 (−OCH$_3$), 3.48 (C5-ring CH), 2.55−1.55 (C5-ring 3CH$_2$), 0.31 (s, 1.1H, PdCH$_3$), 0.11 (s, 6.2H, PdCH$_3$), −0.32 (s, 2H, PdCH$_3$). ^{31}P NMR (CD_2Cl_2): δ 51.1. CI/ESI-HRMS (m/z): Calcd for $[C_{76}H_{50}B_2F_{30}O_{10}P_2Pd_2S_2 + Li]^+$: 2059.0252. Found: 2059.0730.

From 4b. The reaction of **4b** (0.010 g, 9.7 μmol) and $B(C_6F_5)_3$ (0.100 g, 19.4 μmol) in CD_2Cl_2 afforded **5b** quantitatively by NMR.

{(2b-B(C$_6$F$_5$)$_3$)PdMe(Et$_2$O)·Et$_2$O (6b·Et$_2$O). Crystals of **6b**·Et$_2$O were obtained from a concentrated Et$_2$O solution of **5b** at −40 °C. Drying **6b**·Et$_2$O under vacuum for 48 h, sublimation from a frozen benzene solution, and freeze/thaw/pumping the crystals to remove the equivalent of free Et$_2$O resulted in significant decomposition. ^{1}H NMR (CD_2Cl_2): 7.61 (m, 2H, ArH), 7.12 (m, 4H, ArH), 7.06 (m, 2H, ArH), 4.03 (−OCH$_3$), 3.33 (−OCH$_3$), 3.52 (free Et$_2$O and Pd−OEt$_2$), 2.15 (C5-ring 3CH$_2$), 1.83 (C5-ring 3CH$_2$), 1.65 (C5-ring 3CH$_2$), 1.29 (free Et$_2$O and Pd−OEt$_2$), 0.23 (s, PdCH$_3$). ^{31}P NMR (CD_2Cl_2): δ 49.9. ESI-HRMS (m/z): Calcd for $[C_{24}H_{35}O_6PPdS + H]^+$: 1101.0854. Found: 1101.0663.

Reaction of 4b with Excess Ethylene. An NMR tube was charged with **4b** (15 mg, 0.030 mmol Pd$_1$), ferrocene (6.0 mg, 0.030 mmol, internal standard), and $CDCl_2CDCl_2$ (0.5 mL). Ethylene (12 equiv vs Pd) was added by vacuum transfer at −78 °C. The tube was shaken to form a yellow solution of (**2b**)PdMe(C_2H_4) (**7b**). NMR spectra were recorded at −10 °C. The numbering scheme for **7b** is shown in Figure 14. ^{1}H NMR ($CDCl_2CDCl_2$): δ 7.60−6.60 (br, 8H),

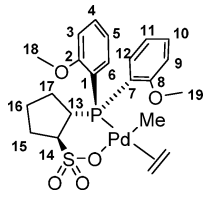

Figure 14. Numbering scheme for **7b**.

5.44 (br s, free and coordinated C_2H_4), 3.90 (br s, 4H, −OCH$_3$ and H[13]), 3.70 (br s, 3H, −OCH$_3$), 3.00 (br s, 1H, H[14]), 2.40−1.80 (6H, H[15−17]), 0.090 (br s, 3H, PdCH$_3$). ^{13}C{^{1}H} NMR ($CDCl_2CDCl_2$): δ 160.2 (C[3] or C[8]), 159.2 (C[3] or C[8]), 140.0−135.0 (C[6] and C[12]), 134.6 (C[10]), 133.0 (C[4]), 123.2 (br, coordinated and free C_2H_4), 121.2 (C[5] and C[11]), 116.1 (C[1] or C[7]), 113.2 (C[1] or C[7]), 110.9 (C[3] or C[9]), 110.2 (C[3] or C[9]), 66.2 (C[14]), 55.6 (C[18]), 55.2 (C[19]), 40.1 ($^1J_{PC}$ = 28 Hz, C[13]), 30.6 (C[17]), 29.7 (C[15]), 26.1 (C[16]), 1.02 (s, PdCH$_3$). ^{31}P{^{1}H} NMR ($CDCl_2CDCl_2$): δ 36.2 (s). The tube was warmed to 5 °C, and ethylene insertion was observed by ^{1}H NMR. After 65 min, a white precipitate had formed.

Ethylene Homopolymerization. Polymerizations were performed in a 300 mL Parr stainless-steel autoclave fitted with a 200 mL glass autoclave liner and equipped with a mechanical stirrer, thermocouple, and water cooling loop and controlled by a Parr 4842 controller. Where indicated, a 10 mL stainless-steel injection tube with valves and Swagelok fittings on both ends was used to inject the catalyst solution into the autoclave after pressurization with ethylene.

Catalyst Injection Procedure. A glass liner was charged with toluene (40 mL) and placed in the autoclave. The catalyst was dissolved in chlorobenzene (10 mL), and the solution was sealed in the injection tube. The autoclave and injection tube were sealed and removed from the glovebox. The autoclave was connected to an ethylene line, stirring initiated at 170 rpm, and the autoclave heated to 80 °C for 20 min. The autoclave was pressurized with ethylene (typically 240 psi). After 10 min, the ethylene line was closed. One end of the injection tube was attached to the autoclave, and the other end was attached to a nitrogen line. The line between the nitrogen tank and the injection tube was evacuated and filled three times with N_2 at a pressure ca. 20 psi higher than the ethylene pressure (typically 260 psi). The catalyst solution was injected into the autoclave. The N_2 injection line was closed. The ethylene line was reopened to the autoclave at a pressure ca. 10 psi higher than the N_2 pressure used (typically 270 psi). After the listed polymerization time (typically 2 h), the ethylene line was closed, and the autoclave was cooled to 25 °C by the cooling loop and an external ice bath, and vented. The polymer was precipitated by addition of acetone (50 mL), collected by filtration, washed with acetone, and dried in a vacuum oven overnight.

Noninjection Procedure. The catalyst was weighed directly into a glass liner or added as a stock solution in dichloromethane (1 mL) and dried under vacuum. Toluene (50 mL) was added, and the liner was placed in the autoclave. The autoclave was sealed and removed from the glovebox and attached to an ethylene line. Stirring was initiated at 160 rpm and the autoclave was heated to 80 °C. The autoclave was pressurized with ethylene. After the listed polymerization time (typically 2 h), the ethylene line was closed and the autoclave was cooled to 25 °C by the cooling loop and an external ice bath, and vented. The polymer was precipitated by addition of acetone (50 mL), collected by filtration, washed with acetone, and dried in a vacuum oven overnight.

Copolymerization of Ethylene and Methyl Acrylate. *Injection Procedure.* The injection procedure for ethylene homopolymerization

DOI: 10.1021/acs.organomet.7b00572
Organometallics 2017, 36, 3415−3428

described above was used with the following modifications: (i) The glass autoclave liner was charged with toluene, BHT (typically 100 mg), and methyl acrylate (total volume 40 mL). (ii) The contents of the autoclave were stirred at 160 rpm. (iii) The autoclave was pressurized with ethylene (380 psi). (iv) The solution of catalyst in 10 mL of chlorobenzene was injected at 400 psi N_2. (v) The autoclave was pressurized with ethylene (420 psi). (vi) MeOH (200 mL) was added to precipitate the polymer.

Noninjection Procedure. The noninjection procedure described above was used with the following modifications: (i) The glass liner was charged with the catalyst stock solution in chlorobenzene (10 mL), BHT (typically 100 mg), and toluene and methyl acrylate to give a total volume of 50 mL. (ii) The contents of the autoclave were stirred at 160 rpm. (iii) The autoclave was pressurized with ethylene (400 psi). (iv) MeOH (200 mL) was added to precipitate the polymer.

Copolymerization of Ethylene and Vinyl Fluoride. *Injection Procedure.* The injection procedure for ethylene homopolymerization was used with the following modifications: (i) The autoclave was pressurized with vinyl fluoride (80 psi) and ethylene (300 psi). (ii) The solution of catalyst in chlorobenzene (10 mL) was injected with N_2 (400 psi). (iii) The autoclave was pressurized with ethylene (410 psi).

Noninjection Procedure. The noninjection procedure for ethylene homopolymerization was used with the following modification: The autoclave was pressurized with vinyl fluoride (80 psi) and ethylene (300 psi).

Polymer Characterization. Gel permeation chromatography (GPC) was performed on a Polymer Laboratories PL−GPC 200 instrument at 150 °C with 1,2,4-trichlorobenzene (stabilized with 125 ppm BHT) as the mobile phase. Three PLgel 10 μm Mixed-B LS columns were used. The molecular weights were calibrated using narrow polystyrene standards with a 10-point calibration of M_n from 570 Da to 5670 kDa, and are corrected for linear polyethylene by universal calibration by using the following Mark−Houwink parameters: polystyrene, $K = 1.75 \times 10^{-2}$ cm^3 g^{-1}, $\alpha = 0.67$; polyethylene, $K = 5.90 \times 10^{-2}$ cm^3 g^{-1}, $\alpha = 0.69$.[83] DSC measurements were performed on a TA Instruments 2920 differential scanning calorimeter. Samples (5 mg) were annealed by heating to 180 °C at 15 C/min, cooled to 50 °C at 15 °C/min, and analyzed by heating to 180 °C at 15 °C/min. NMR assignments for polymers and copolymers are based on literature sources.[5,16,19,57,62,84,85]

DFT Calculations. Geometry optimization and frequency calculations were completed using Gaussian09.[86] All calculations were done using the B3LYP functional with the LANL2DZ effective core potential on Pd and the 6-31G(d) basis set on all other atoms. All energy differences were calculated from the sum of the electronic and thermal free energies (ε 0 + G corr) for each respective species.

■ ASSOCIATED CONTENT

Supporting Information

The Supporting Information is available free of charge on the ACS Publications website at DOI: 10.1021/acs.organomet.7b00572.

Additional experimental procedures, NMR data for compounds and polymers, supporting figures and tables, and detailed computational results (PDF)

Cartesian coordinates of optimized DFT structures (XYZ)

Accession Codes

CCDC 1557502−1557509 contain the supplementary crystallographic data for this paper. These data can be obtained free of charge via www.ccdc.cam.ac.uk/data_request/cif, or by emailing data_request@ccdc.cam.ac.uk, or by contacting The Cambridge Crystallographic Data Centre, 12 Union Road, Cambridge CB2 1EZ, UK; fax: +44 1223 336033.

■ AUTHOR INFORMATION

Corresponding Author

*E-mail: rfjordan@uchicago.edu.

ORCID

Richard F. Jordan: 0000-0002-3158-4745

Notes

The authors declare no competing financial interest.

■ ACKNOWLEDGMENTS

This work was supported by the National Science Foundation through grants CHE-0911180, CHE-1709159, and CHE-1048528 (CRIF MU Instrumentation) and the U.S. Department of Education through grant P200A120093. This work used the Extreme Science and Engineering Discovery Environment (XSEDE),[87] which is supported by National Science Foundation grant number ACI-1548562. This work also used the Advanced Photon Source, an Office of Science User Facility operated for the U.S. Department of Energy (DOE) Office of Science by Argonne National Laboratory, which was supported by the U.S. DOE under Contract No. DE-AC02-06CH11357. ChemMatCARS Sector 15 at Argonne National Laboratory is principally supported by the Divisions of Chemistry (CHE) and Materials Research (DMR), National Science Foundation, under grant number NSF/CHE-1346572. We thank Antoni Jurkiewicz for assistance with NMR spectroscopy, Chang-Jin Qin for assistance with mass spectrometry, Alexander Filatov and Ian Steele for assistance with X-ray crystallography, and Erik Reinhart for assistance with DFT calculations.

■ REFERENCES

(1) Nakamura, A.; Ito, S.; Nozaki, K. *Chem. Rev.* **2009**, *109*, 5215−5244.

(2) Ito, S.; Nozaki, K. *Chem. Rec.* **2010**, *10*, 315−325.

(3) Nakamura, A.; Anselment, T. M. J.; Claverie, J.; Goodall, B.; Jordan, R. F.; Mecking, S.; Rieger, B.; Sen, A.; van Leeuwen, P. W. N. M.; Nozaki, K. *Acc. Chem. Res.* **2013**, *46*, 1438−1449.

(4) Franssen, N. M. G.; Reek, J. N. H.; de Bruin, B. *Chem. Soc. Rev.* **2013**, *42*, 5809−5832.

(5) Drent, E.; van Dijk, R.; van Ginkel, R.; van Oort, B.; Pugh, R. I. *Chem. Commun.* **2002**, 744−745.

(6) Guironnet, D.; Roesle, P.; Rünzi, T.; Göttker-Schnetmann, I.; Mecking, S. *J. Am. Chem. Soc.* **2009**, *131*, 422−423.

(7) Kochi, T.; Nakamura, A.; Ida, H.; Nozaki, K. *J. Am. Chem. Soc.* **2007**, *129*, 7770−7771.

(8) Luo, S.; Vela, J.; Lief, G. R.; Jordan, R. F. *J. Am. Chem. Soc.* **2007**, *129*, 8946−8947.

(9) Ito, S.; Munakata, K.; Nakamura, A.; Nozaki, K. *J. Am. Chem. Soc.* **2009**, *131*, 14606−14607.

(10) Weng, W.; Shen, Z.; Jordan, R. F. *J. Am. Chem. Soc.* **2007**, *129*, 15450−15451.

(11) Leicht, H.; Göttker-Schnetmann, I.; Mecking, S. *Angew. Chem., Int. Ed.* **2013**, *52*, 3963−3966.

(12) Borkar, S.; Newsham, D. K.; Sen, A. *Organometallics* **2008**, *27*, 3331−3334.

(13) Skupov, K. M.; Piche, L.; Claverie, J. P. *Macromolecules* **2008**, *41*, 2309−2310.

(14) Ota, Y.; Ito, S.; Kuroda, J.; Okumura, Y.; Nozaki, K. *J. Am. Chem. Soc.* **2014**, *136*, 11898−11901.

(15) Jian, Z.; Wucher, P.; Mecking, S. *Organometallics* **2014**, *33*, 2879−2888.

(16) Contrella, N. D.; Sampson, J. R.; Jordan, R. F. *Organometallics* **2014**, *33*, 3546−3555.

(17) Neuwald, B.; Falivene, L.; Caporaso, L.; Cavallo, L.; Mecking, S. *Chem. - Eur. J.* **2013**, *19*, 17773−17788.

DOI: 10.1021/acs.organomet.7b00572
Organometallics 2017, 36, 3415−3428

(18) Neuwald, B.; Caporaso, L.; Cavallo, L.; Mecking, S. *J. Am. Chem. Soc.* **2013**, *135*, 1026−1036.
(19) Wada, S.; Jordan, R. F. *Angew. Chem., Int. Ed.* **2017**, *56*, 1820−1824.
(20) Britovsek, G. J. P.; Gibson, V. C.; Wass, D. F. *Angew. Chem., Int. Ed.* **1999**, *38*, 428−447.
(21) Gibson, V. C.; Spitzmesser, S. K. *Chem. Rev.* **2003**, *103*, 283.
(22) Piche, L.; Daigle, J. C.; Rehse, G.; Claverie, J. P. *Chem. - Eur. J.* **2012**, *18*, 3277−3285.
(23) Piche, L.; Daigle, J.-C.; Poli, R.; Claverie, J. P. *Eur. J. Inorg. Chem.* **2010**, *2010*, 4595−4601.
(24) Wucher, P.; Goldbach, V.; Mecking, S. *Organometallics* **2013**, *32*, 4516−4522.
(25) Jover, J.; Fey, N.; Harvey, J. N.; Lloyd-Jones, G. C.; Orpen, A. G.; Owen-Smith, G. J. J.; Murray, P.; Hose, D. R. J.; Osborne, R.; Purdie, M. *Organometallics* **2010**, *29*, 6245−6258.
(26) Replacement of the arene linker with an alkane linker will enhance the donor ability of the phosphine and sulfonate group. The Tolman electronic parameter for P(2-OMe-Ph)$_2$(*m*-tolyl) (2061.6 cm^{-1}) is larger than that for P(2-OMe-Ph)$_2$Cy (2058 cm^{-1}). Alkanesulfonates are 1−2 pK_a units more basic than aryl sulfonates (e.g., pK_a: PhSO$_3$H −2.8, EtSO$_3$H −1.8). A small alkane linker should not exert significant steric effects, while a bulky alkane linker may influence the conformation of the −PR$_2$ units.
(27) Paetzold, E.; Kinting, A.; Oehme, G. *J. Prakt. Chem.* **1987**, *329*, 725−731.
(28) Ganguly, S.; Mague, J. T.; Roundhill, D. M. *Inorg. Chem.* **1992**, *31*, 3500−3501.
(29) García Suárez, E. J.; Ruiz, A.; Castillón, S.; Oberhauser, W.; Bianchini, C.; Claver, C. *Dalton Trans.* **2007**, 2859−2861.
(30) Lu, J.; Ye, J.; Duan, W.-L. *Org. Lett.* **2013**, *15*, 5016−5019.
(31) Bettucci, L.; Bianchini, C.; Claver, C.; Suarez, E. J. G.; Ruiz, A.; Meli, A.; Oberhauser, W. *Dalton Trans.* **2007**, 5590−5602.
(32) Feng, G.; Conley, M. P.; Jordan, R. F. *Organometallics* **2014**, *33*, 4486−4496.
(33) Rotation around the C−S bond before recoordination will permute the Pd-coordinated and terminal oxygens.
(34) Noda, S.; Nakamura, A.; Kochi, T.; Chung, L. W.; Morokuma, K.; Nozaki, K. *J. Am. Chem. Soc.* **2009**, *131*, 14088−14100.
(35) Conley, M. P.; Jordan, R. F. *Angew. Chem., Int. Ed.* **2011**, *50*, 3744−3746.
(36) Cai, Z.; Shen, Z.; Zhou, X.; Jordan, R. F. *ACS Catal.* **2012**, *2*, 1187−1195.
(37) Bakker, B.; Cerfontain, H.; Tomassen, H. *J. Org. Chem.* **1989**, *54*, 1680−1684.
(38) Wife, R. L.; Van Oort, A. B.; Van Doorn, J. A.; Van Leeuwen, P. W. N. M. *Synthesis* **1983**, *1983*, 71−73.
(39) Aspinall, H. C.; Moore, S. R.; Smith, A. K. *J. Chem. Soc., Dalton Trans.* **1993**, 993−996.
(40) Bianchini, C.; Lenoble, G.; Oberhauser, W.; Parisel, S.; Zanobini, F. *Eur. J. Inorg. Chem.* **2005**, *2005*, 4794−4800.
(41) Aspinall, H. C.; Tillotson, M. R. *Inorg. Chem.* **1996**, *35*, 5−8.
(42) Miljkovic, M. In *Carbohydrates: Synthesis, Mechanisms, and Stereoelectronic Effects*; Springer: New York, 2009; pp 169−190.
(43) Newsham, D. K.; Borkar, S.; Sen, A.; Conner, D. M.; Goodall, B. L. *Organometallics* **2007**, *26*, 3636−3638.
(44) The N−Pd−O angles in **3a,b** are 2−4° larger and the O−Pd−P angles are 2−4° smaller than in **3c,d**.
(45) Howell, J. A. S.; Palin, M. G.; Yates, P. C.; McArdle, P.; Cunningham, D.; Goldschmidt, Z.; Gottlieb, H. E.; Hezroni-Langerman, D. *J. Chem. Soc., Perkin Trans. 2* **1992**, 1769−1775.
(46) Howell, J. A. S.; Fey, N.; Lovatt, J. D.; Yates, P. C.; McArdle, P.; Cunningham, D.; Sadeh, E.; Gottlieb, H. E.; Goldschmidt, Z.; Hursthouse, M. B.; Light, M. E. *J. Chem. Soc., Dalton Trans.* **1999**, 3015−3028.
(47) Another metric that can be used to compare the puckering in **3a,b** and **3c,d** is the distance between the O−Pd−P plane and the S atom and two C atoms within the chelate ring. These distances are as follows: **3a**: 1.030, 1.661, and 0.507 Å; **3c**: 0.565, −0.477, and −0.656 Å; **3b**: 1.099, 1.964, and 1.032 Å; **3d**: 0.485, −0.518, and −0.654 Å. These data confirm that the chelate rings of **3a,b** are more puckered than those in **3c,d**.
(48) Sundquist, W. I.; Bancroft, D. P.; Lippard, S. J. *J. Am. Chem. Soc.* **1990**, *112*, 1590−1596.
(49) Mukhopadhyay, A.; Pal, S. *Eur. J. Inorg. Chem.* **2006**, *2006*, 4879−4887.
(50) Buckingham, A. D.; Stephens, P. J. *J. Chem. Soc.* **1964**, 4583−4587.
(51) Miller, R. G.; Stauffer, R. D.; Fahey, D. R.; Parnell, D. R. *J. Am. Chem. Soc.* **1970**, *92*, 1511−1521.
(52) Brookhart, M.; Green, M. L. H.; Parkin, G. *Proc. Natl. Acad. Sci. U. S. A.* **2007**, *104*, 6908−6914.
(53) Zhang, Y.; Lewis, J. C.; Bergman, R. G.; Ellman, J. A.; Oldfield, E. *Organometallics* **2006**, *25*, 3515−3519.
(54) Lau, K. C.; Petro, B. J.; Bontemps, S.; Jordan, R. F. *Organometallics* **2013**, *32*, 6895−6898.
(55) Wucher, P.; Roesle, P.; Falivene, L.; Cavallo, L.; Caporaso, L.; Göttker-Schnetmann, I.; Mecking, S. *Organometallics* **2012**, *31*, 8505−8515.
(56) Wucher, P.; Caporaso, L.; Roesle, P.; Ragone, F.; Cavallo, L.; Mecking, S.; Göttker-Schnetmann, I. *Proc. Natl. Acad. Sci. U. S. A.* **2011**, *108*, 8955−8959.
(57) Rünzi, T.; Guironnet, D.; Göttker-Schnetmann, I.; Mecking, S. *J. Am. Chem. Soc.* **2010**, *132*, 16623−16630.
(58) Still, W. C.; Galynker, I. *Tetrahedron* **1981**, *37*, 3981−3996.
(59) Anet, F. A. L. In *Dynamic Chemistry*; Springer Berlin Heidelberg: Berlin, Heidelberg, 1974; pp 169−220.
(60) Replacing an H atom in CH$_2$Cl$_2$ with a −CHCl$_2$ unit is expected to decrease the pK_a by ca. 2 units based on pK_a trends for the analogous carboxylic acids. For example, the pK_a of CCl$_2$HCO$_2$H (1.35) is 2.42 units lower than that of HCO$_2$H (3.77).
(61) The Abraham parameter $\Sigma\alpha_2^H$ describes the hydrogen-bond acidity of a molecule. The $\Sigma\alpha_2^H$ value for CHCl$_2$CHCl$_2$ (0.18) is larger than that of CH$_2$Cl$_2$ (0.10), indicating that the former is a better hydrogen bond donor. Value for CH$_2$Cl$_2$: Abraham, M. *Chem. Soc. Rev.* **1993**, *22*, 73−83. Value for CHCl$_2$CHCl$_2$: *ACD/Labs I-Lab 2.0, Algorithm* v5.0.0.184; ACD/Labs: Toronto, Ontario, Canada, 2016.
(62) Vela, J.; Lief, G. R.; Shen, Z.; Jordan, R. F. *Organometallics* **2007**, *26*, 6624−6635.
(63) Stereoisomers that differ in the configurations of the S atoms are also possible for **4b**. However, the isolation of *SS,RR*-**5b** from the reaction of **4b** with B(C$_6$F$_5$)$_3$ suggests that the two isomers of **4b** differ in the relative configurations of the cyclopentane rings.
(64) Compound **3a** generates only a trace amount of PE at 80 °C, consistent with the low thermal stability of this complex.
(65) Skupov, K. M.; Marella, P. R.; Simard, M.; Yap, G. P. A.; Allen, N.; Conner, D.; Goodall, B. L.; Claverie, J. P. *Macromol. Rapid Commun.* **2007**, *28*, 2033−2038.
(66) Berkefeld, A.; Mecking, S. *Angew. Chem., Int. Ed.* **2008**, *47*, 2538−2542.
(67) Nakano, R.; Chung, L. W.; Watanabe, Y.; Okuno, Y.; Okumura, Y.; Ito, S.; Morokuma, K.; Nozaki, K. *ACS Catal.* **2016**, *6*, 6101−6113.
(68) Stack, G. M.; Mandelkern, L.; Voigt-Martin, I. G. *Macromolecules* **1984**, *17*, 321−331.
(69) Mandelkern, L.; Prasad, A.; Alamo, R. G.; Stack, G. M. *Macromolecules* **1990**, *23*, 3696−3700.
(70) Prasad, A.; Mandelkern, L. *Macromolecules* **1989**, *22*, 914−920.
(71) Skupov, K. M.; Hobbs, J.; Marella, P.; Conner, D.; Golisz, S.; Goodall, B. L.; Claverie, J. P. *Macromolecules* **2009**, *42*, 6953−6963.
(72) Shen, Z.; Jordan, R. F. *Macromolecules* **2010**, *43*, 8706−8708.
(73) Solubility limitations for **4b** limited experiments to CDCl$_2$CDCl$_2$, which freezes at −44 °C, precluding studies at lower temperatures.
(74) The observed activity of ca. 200 kg mol$_{Pd}^{-1}$ h^{-1} (Table 1) at 80 °C corresponds to a turnover frequency of 2 s^{-1} and a free energy barrier of $\Delta G^{\ddagger}_{insert}$ = 20 kcal/mol. The $\Delta G^{\ddagger}_{insert}$ values estimated by NMR at 5 °C and from the polymerization activity at 80 °C are

DOI: 10.1021/acs.organomet.7b00572
Organometallics 2017, 36, 3415−3428

expected to be similar, as $\Delta S^{\ddagger}_{insert}$ is expected to be small for this unimolecular process.
(75) Haras, A.; Anderson, G. D. W.; Michalak, A.; Rieger, B.; Ziegler, T. *Organometallics* **2006**, *25*, 4491−4497.
(76) Haras, A.; Michalak, A.; Rieger, B.; Ziegler, T. *Organometallics* **2006**, *25*, 946−953.
(77) Nozaki, K.; Kusumoto, S.; Noda, S.; Kochi, T.; Chung, L. W.; Morokuma, K. *J. Am. Chem. Soc.* **2010**, *132*, 16030−16042.
(78) Zhou, X.; Lau, K.-C.; Petro, B. J.; Jordan, R. F. *Organometallics* **2014**, *33*, 7209−7214.
(79) For other cases in which cis/trans isomerization or equivalent exchange processes are mediated by intramolecular coordination of hemilabile ligands, see: Rotondo, E.; Battaglia, G.; Arena, C. G.; Faraone, F. *J. Organomet. Chem.* **1991**, *419*, 399−402. Imhoff, P.; van Asselt, R.; Ernsting, J. M.; Vrieze, K.; Elsevier, C. J.; Smeets, W. J. J.; Spek, A. L.; Kentgens, A. P. M. *Organometallics* **1993**, *12*, 1523−1536. Casares, J. A.; Espinet, P. *Inorg. Chem.* **1997**, *36*, 5428−5431.
(80) Cotton, A. F.; Wilkinson, G.; Murillo, C. A.; Bochmann, M. In *Advanced Inorganic Chemistry*; Wiley-Interscience: New York, 1999; pp 521−522.
(81) Rulke, R. E.; Ernsting, J. M.; Spek, A. L.; Elsevier, C. J.; van Leeuwen, P. W. N. M.; Vrieze, K. *Inorg. Chem.* **1993**, *32*, 5769−5778.
(82) De Graaf, W.; Boersma, J.; Smeets, W. J. J.; Spek, A. L.; Van Koten, G. *Organometallics* **1989**, *8*, 2907−2917.
(83) Grinshpun, V.; Rudin, A. *Makromol. Chem., Rapid Commun.* **1985**, *6*, 219−223.
(84) Daigle, J.-C.; Piche, L.; Claverie, J. P. *Macromolecules* **2011**, *44*, 1760−1762.
(85) Galland, G. B.; de Souza, R. F.; Mauler, R. S.; Nunes, F. F. *Macromolecules* **1999**, *32*, 1620−1625.
(86) Frisch, M. J.; Trucks, G. W.; Schlegel, H. B.; Scuseria, G. E.; Robb, M. A.; Cheeseman, J. R.; Scalmani, G.; Barone, V.; Mennucci, B.; Petersson, G. A.; Nakatsuji, H.; Caricato, M.; Li, X.; Hratchian, H. P.; Izmaylov, A. F.; Bloino, J.; Zheng, G.; Sonnenberg, J. L.; Hada, M.; Ehara, M.; Toyota, K.; Fukuda, R.; Hasegawa, J.; Ishida, M.; Nakajima, T.; Honda, Y.; Kitao, O.; Nakai, H.; Vreven, T.; Montgomery, J. A., Jr.; Peralta, J. E.; Ogliaro, F.; Bearpark, M.; Heyd, J. J.; Brothers, E.; Kudin, K. N.; Staroverov, V. N.; Kobayashi, R.; Normand, J.; Raghavachari, K.; Rendell, A.; Burant, J. C.; Iyengar, S. S.; Tomasi, J.; Cossi, M.; Rega, N.; Millam, J. M.; Klene, M.; Knox, J. E.; Cross, J. B.; Bakken, V.; Adamo, C.; Jaramillo, J.; Gomperts, R.; Stratmann, R. E.; Yazyev, O.; Austin, A. J.; Cammi, R.; Pomelli, C.; Ochterski, J. W.; Martin, R. L.; Morokuma, K.; Zakrzewski, V. G.; Voth, G. A.; Salvador, P.; Dannenberg, J. J.; Dapprich, S.; Daniels, A. D.; Farkas, O.; Foresman, J. B.; Ortiz, J. V.; Cioslowski, J.; Fox, D. J. *Gaussian 09*, revision A.02; Gaussian, Inc.: Wallingford, CT, 2009.
(87) Towns, J.; Cockerill, T.; Dahan, M.; Foster, I.; Gaither, K.; Grimshaw, A.; Hazlewood, V.; Lathrop, S.; Lifka, D.; Peterson, G. D.; Roskies, R.; Scott, J. R.; Wilkens-Diehr, N. *Comput. Sci. Eng.* **2014**, *16*, 62−74.

DOI: 10.1021/acs.organomet.7b00572
Organometallics 2017, 36, 3415−3428